

Citation for published version:

Shen, J, Jeihanipour, A, Richards, BS & Schäfer, Al 2019, 'Renewable energy powered membrane technology: Experimental investigation of system performance with variable module size and fluctuating energy', *Separation and Purification Technology*, vol. 221, pp. 64-73. https://doi.org/10.1016/j.seppur.2019.03.004

DOI:

10.1016/j.seppur.2019.03.004

Publication date: 2019

Document Version
Peer reviewed version

Link to publication

Publisher Rights CC BY-NC-ND

## **University of Bath**

## **Alternative formats**

If you require this document in an alternative format, please contact: openaccess@bath.ac.uk

**General rights** 

Copyright and moral rights for the publications made accessible in the public portal are retained by the authors and/or other copyright owners and it is a condition of accessing publications that users recognise and abide by the legal requirements associated with these rights.

Take down policy

If you believe that this document breaches copyright please contact us providing details, and we will remove access to the work immediately and investigate your claim.

Download date: 07. Mar. 2023

1	Renewable energy powered membrane technology:						
2	experimental investigation of system performance with						
3	variable module size and fluctuating energy						
4							
5	Junjie Shen <sup>1,2,3</sup> , Azam Jeihanipour⁴, Bryce S. Richards <sup>2,4</sup> , Andrea I. Schäfer <sup>3,5*</sup>						
6							
7	<sup>1</sup> Centre for Advanced Separations Engineering, University of Bath, Bath BA2 7AY,						
8	United Kingdom						
9	<sup>2</sup> School of Engineering and Physical Sciences, Heriot-Watt University, Edinburgh						
10	EH14 4AS, United Kingdom						
11	<sup>3</sup> Water and Environmental Science and Engineering, Nelson Mandela African Institute of Science						
12	and Technology, Arusha, Tanzania						
13	<sup>4</sup> Institute of Microstructure Technology (IMT), KIT, Hermann-von-Helmholtz-Platz 1, 76344						
14	Eggenstein-Leopoldshafen, Germany						
15	<sup>5</sup> Membrane Technology Department, Institute of Functional Interfaces (IFG-MT), Karlsruhe						
16	Institute of Technology, Hermann-von-Helmholtz-Platz 1,						
17	76344 Eggenstein-Leopoldshafen, Germany						
18							
19							
20	Separation and Purification Technology						
21							
22	Submitted 9 April 2018						
23	Resubmitted 12 November 2018 & 2 March 2019						
24							
25							
26							
27							
28							
29							
30							
31							
32	*corresponding author: Prof. Andrea I. Schäfer, +49 (0)721 608 26906						
33	Andrea.Iris.Schaefer@kit.edu						

# Abstract

34

35

36

37

38

39

40

41

42

43

44

45

46

47

48

49

50

51

52

53

Integration of renewable energy and membrane filtration technologies such as nanofiltration (NF) and reverse osmosis (RO) can provide drinking water in places where freshwater is scarce and grid electrical connections are unavailable. This study investigated a directly-connected photovoltaicpowered membrane system under fluctuating solar conditions. Specifically, two configurations of NF/RO membranes with the same membrane area were investigated: a) 1× 4" module, which contained one 4" NF/RO element; and b) 3× 2.5" module, which contained three 2.5" NF/RO elements in series. A high fluoride brackish water ([F-] = 56.2 mg/L, total dissolved solids [TDS] = 4076 mg/L) collected from northern Tanzania was treated by different membranes in the two configurations. Performance indicators such as flux, specific energy consumption, and permeate Fconcentration were monitored over a 60-min period of energy fluctuation that are part of a typical solar day. The results showed that the overall performance of the 1× 4" module was superior to that of the 3× 2.5" module. This is because the performance of a 3× 2.5" module degraded significantly from the first element to the third element due to the increased feed concentration and the decreased net driving pressure. Three 1×4" modules (BW30, BW30LE and NF90) and one 3×2.5" module (BW30) were able to meet the drinking water guideline for fluoride. During cloud periods, the transient permeate F<sup>-</sup> concentration exceeded the guideline value due to insufficient power, however the cumulative permeate F- concentration was always well below the guideline. The photovoltaicpowered membrane system equipped with the above modules provides a promising solution for addressing drinking water problems in remote and rural areas.

54

55

- **Keywords:** brackish water; desalination; module size; fluoride; energy fluctuation; nanofiltration;
- 57 reverse osmosis

5859

## 1. Introduction

The ever-increasing demand for fresh water and clean energy are among the major issues that humans will face and need to solve in the 21st century [1]. The two issues are intertwined via the energy-water nexus, meaning here that drinking water treatment and supply will always require energy [2]. Extreme cases can be found in the many remote locations in both developed and developing countries, which are far away from both centralized water and grid electricity supplies, and where natural freshwater resources are scarce as well [3, 4]. In such cases, the integration of renewable energy (RE) technologies with membrane filtration technologies, namely nanofiltration (NF) and reverse osmosis (RO), provides a sustainable solution for this issue [3-5]. For example, many photovoltaic (PV) powered membrane systems have been successfully implemented throughout the world [6-10]. The figure-of-merit for system performance is typically the specific energy consumption (SEC, units: kWh/m³), which represents how much electricity is required to produce 1 m³ of clean drinking water. The SEC is dependent on feed water salinity, system size, and membrane type [3, 11].

In most PV-powered membrane systems, batteries are used to compensate for variations in solar irradiance [6, 8, 12, 13]. Nevertheless, batteries exhibit several disadvantages such as reducing the overall system efficiency, high capital and maintenance costs, and potential negative environmental impacts in case of improper disposal [7, 14]. Therefore, it has been suggested to avoid the use of batteries in such membrane systems to increase the efficiency and robustness, while decreasing costs [9, 14-16]. However, in such batteryless systems the DC power produced by the PV modules is directly coupled to the pump motor. The system is naturally subjected to widely varying energy availability, which arises from the Earth's rotation, as well as landscape and weather conditions, such as clouds, wind and ambient temperature [17]. The fluctuating current produced by the PV modules subjects the NF/RO membranes integrated into such systems to fluctuations in pressure and flow rate, which affects their flux and permeate water quality [9, 14, 18]. Additionally, manufacturer of NF/RO membranes typically recommend to operate the membrane system in a constant permeate flow rate to increase the life time of the membrane [19]. Richards et al. [18] investigated the effects of fluctuating energy on retention of dissolved contaminants from real water using a PV-powered NF/RO system. It was found that fluctuations in pressure and feed flow, as a result of variation in solar irradiance, impacted the removal of solutes whose retention mechanism was convection/diffusion. However, solutes that were retained via size exclusion and charge repulsion were not affected by fluctuations in solar energy. It has been shown that when a batteryless PVpowered NF/RO system was working under fluctuating conditions, even though the flux was often low, a satisfactory quality of water at a low SEC could be delivered [17, 20]. Further, there is a potential for the NF/RO membrane to possibly benefit from steps in the solar irradiance due to disruption of the concentration polarization layer via a naturally induced backwash occurring when the pump switched off [17].

Currently, spiral wound (SW) modules are the most widely used membrane modules for NF/RO, thanks to their large membrane packing area, high design flexibility, and manufacturability [21]. The construction of a typical SW module can be found in Figure S1. The basic component in a SW module is membrane envelope, which is made of two flat-sheet membranes sealed on three edges, with a permeate carrier filled in between [22, 23]. The achievable performance of a SW module depends not only on the physicochemical characteristics of membrane active surface, but also on the module size parameters, such as membrane envelope number and membrane dimensions [22, 24]. However, there has been little research conducted on the effect of module size on batteryless PVpowered membrane systems. Knowledge of the performance of different module sizes under energyfluctuating conditions is needed for system planning and design, especially for remote and developing areas. It should be noted that during operation with fluctuating energy feed flow and transmembrane pressure vary. This means that pressure drop, concentration polarization (and with this the osmotic pressure at the membrane surface) vary significantly more than in conventionally operated membrane systems. Further, the availability of direct current (DC) equipment such as pumps that are suitable for small systems remains limited. In a scenario where salinity is high, rejection is high and permeability is good and the pressure that can be supplied by the pump is limited, the osmotic pressure may exceed the applied pressure and water permeation is no longer possible. This is typically most likely to happen at the outlet of the module, while during fluctuation this scenario may be more common. In consequence, the design cannot always maintained ideal and studies are aimed at finding the safe operating window (SOW) for a particular water. Remaining within this SOW is a matter of a suitable control system.

This paper addresses this knowledge gap by utilizing two types of SW modules (with comparable membrane areas) in treating a Tanzanian brackish water with high fluoride contents. In Tanzania, excessive fluoride in drinking water has been recognized to cause large-scale health problems, including dental and skeletal fluorosis [25-27]. Current defluoridation methods available in Tanzania, such as adsorption and precipitation, are far from satisfactory due to insufficient removal capacity and complicated maintenance [28-30]. Previous work from has demonstrated that NF/RO membranes are effective in removing fluoride from natural waters in Tanzania [10, 20, 31]. In this study, a batteryless PV-powered membrane system with two types of SW modules will be operated under energy fluctuations. Variations of operating parameters (pressure, feed flow) and performance indicators (flux, SEC, permeate concentration) of the two modules will be compared. In addition, the

performance degradation of each element within the 3× 2.5" module will be investigated. The concentration polarization of such operation was calculated for three energy levels observed from the experimental study using computational fluid dynamics (CFD) for this variable module configuration to understand the transport phenomena [32].

## 2. Materials and methods

#### 2.1. Water characteristics

A high fluoride content brackish water from a borehole in Mdori, a remote village near Lake Manyara in northern Tanzania (GPS coordinates: S03°47.273', E035°51.138'), was used as natural water to be treated by NF/RO. 5000 L of water was collected by a water truck on 17 January, 2014. The pH and electrical conductivity (EC) were measured by a pH/conductivity meter (Multi 340i, WTW, Germany). Turbidity was measured using a turbidity meter (TN100, Eutech, Netherlands). Total organic carbon (TOC) and inorganic carbon (IC) were determined by a portable TOC analyzer with autosampler (Sievers 900, GE Analytical Instruments, USA). Fluoride ion (F-) was determined by an ion-selective electrode connected to a pH meter (826 pH Mobile Meter, Metrohm, UK). Chloride (Cl<sup>-</sup>) and sulphate (SO<sub>4</sub><sup>2-</sup>) ions were analyzed by an ion chromatograph (IC 790, Metrohm, Germany). Metal and non-metallic elements were measured via inductively coupled plasma optical emission spectrometry (ICP-OES) (Vista-PRO CCD Simultaneous ICP-OES, Varian, Netherlands). Methods of IC and ICP-OES were described by Shen et al. [20]. Total dissolved solid (TDS) was calculated as the sum of major cations and anions.

The water quality components are presented in Table 1. The water was characterized by high alkalinity (pH 9.7) and high salinity (TDS 4076 mg/L), according to the World Health Organization (WHO) guideline for drinking water [33]. The dominant ions were Na<sup>+</sup>, SO<sub>4</sub><sup>2-</sup>, Cl<sup>-</sup>, and IC, including CO<sub>3</sub><sup>2-</sup> and HCO<sub>3</sub><sup>-</sup>. High levels of salinity and turbidity have no health significance, but they reduce the acceptability of drinking water in terms of its taste, odor and appearance [33]. The F<sup>-</sup> concentration was 56.2 mg/L, which exceeded the WHO guideline of 1.5 mg/L by more than 37 times. Such high level of F<sup>-</sup> poses a genuine health risk of dental and skeletal fluorosis [25]. Therefore, F<sup>-</sup>, IC and EC (represents salinity) were the three target components to treat in order to produce acceptable drinking water from the Mdori brackish water.

Parameter	Unit	Value	WHO guideline [33]	
pH (25 °C)	_	9.7		
EC (25 °C)	μS/cm	4940	_	
TDS	mg/L	4076a	1000 <sup>b</sup>	
Turbidity	NTU	15.8	1°	
TOC	mg/L	5.3	_	
IC	mg/L	430.0	_	
F-	mg/L	56.2	1.5	
Cl-	mg/L	268.0	250 <sup>b</sup>	
SO <sub>4</sub> <sup>2-</sup>	mg/L	306.1	250 <sup>b</sup>	
Al	mg/L	0.1	$0.1^{d}$	
В	mg/L	1.9	2.4	
Ca	mg/L	1.6	$300^{b}$	
Fe	mg/L	0.2	$0.3^{\rm b}$	
K	mg/L	16.3	_	
Mg	mg/L	0.5	_	
Na	mg/L	1358.1	$200^{b}$	
P	mg/L	0.7	_	
Si	mg/L	17.3	_	
Sr	mg/L	0.1	_	

<sup>&</sup>lt;sup>a</sup> Calculated as the sum of cations and anions, the charge difference between cations and anions < 5%.

### 2.2. System design and membrane characteristics

An integrated PV-powered membrane system was used for the experiments. The filtration system combines ultrafiltration (UF) and NF/RO processes. The UF stage was used to remove particles, viruses and bacteria while the NF/RO stage was for desalination. A schematic is shown in Figure 1, while full details of the system have been published elsewhere [20, 34, 35]. As part of the design concept this system includes some unusual features; the system is operated at relatively low recovery (10-30%) and there is no energy recovery in the system (in form of a booster pump) that would enhance this recovery. The reason is firstly that very few suitable DC components exist to allow such operation for non-seawater systems. Secondly, provided the water is of such quality that

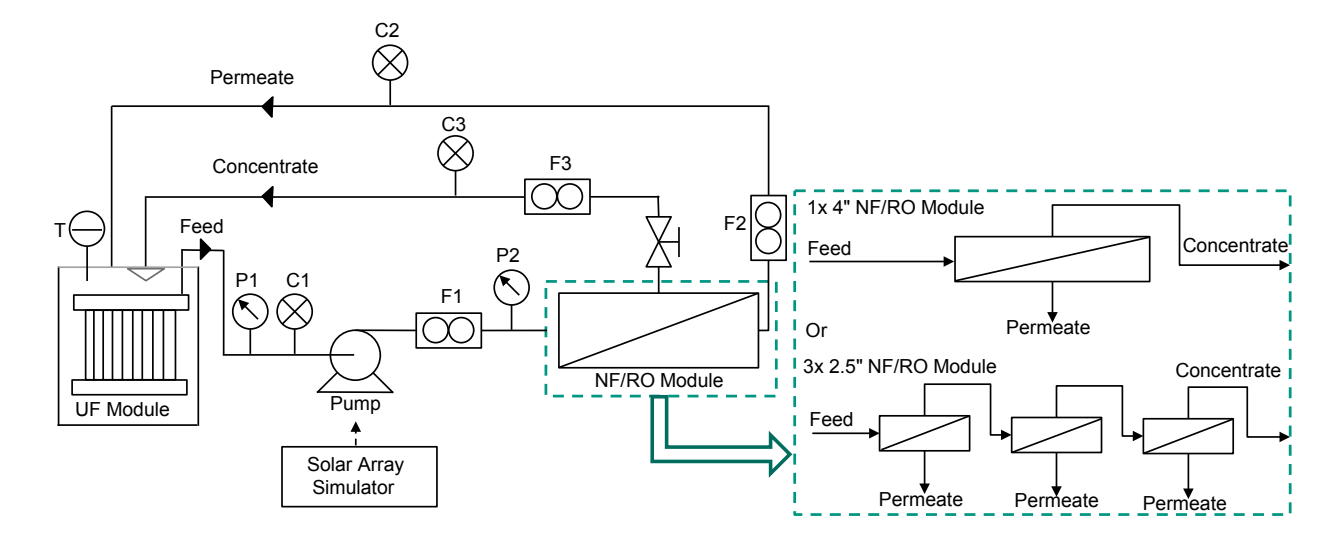
<sup>&</sup>lt;sup>b</sup>Based on average taste thresholds.

<sup>&</sup>lt;sup>c</sup> Based on disinfection effectiveness.

<sup>&</sup>lt;sup>d</sup>Based on optimization of the coagulation process.

after the physical disinfection stage (UF) it can be safely used for washing or showering purposes, then this approach allows to avoid concentrate production. This is highly beneficial in remote areas where no adequate treatment of such concentrates is feasible. In this case this is indeed possible, as the feed water was used for laundry where fluoride is not a concern and the marginal increase in salinity can be tolerated.

The NF/RO elements were spiral wound in 40" (1 m) length and in two different diameters, 2.5" and 4". Two different configurations, or modules, of the NF/RO elements were tested. The first module contained one 4" NF/RO element (denoted as the 1× 4" module), and the second module contained three 2.5" elements in series (denoted as the 3× 2.5" module) such that the concentrate of the first element became the feed to the second, and the concentrate of the second the feed of the third. Therefore, the length of the  $3 \times 2.5$ " module was triple the length of the  $1 \times 4$ " module, while the cross-sectional area of the  $3 \times 2.5''$  module was approximately one-third of that of the  $1 \times 4''$ module. In the 1× 4" module, the permeate and concentrate streams were recirculated into the feed tank; in the  $3 \times 2.5''$  module, the three permeate streams (one from each element) and the concentrate stream of the last element were recirculated to the feed tank, separately. Pressure, temperature, flow rate and EC sensors were installed on the feed, permeate and concentrate streams. The sensor details can be found in a previous publication [35]. As the system was adapted to install the  $3 \times 2.5$ " module in the existing system, no additional pressure sensors were added and hence the pressure drop across the individual modules is not available. This was exacerbated by the concentrate pressure sensor being not fully functional. These are a design and operational shortfalls that could not be remedied during the field work. Data from the sensors were recorded by a datalogger at 2 second intervals and transferred to a laptop using LabVIEW 8.0 software.



176

177

178

179

180

181

182

183

184

185

186

187

188

189

190

191

192

193

194

195

196

197

Figure 1 Schematic of the PV-powered membrane system configurations equipped with either  $1 \times 4''$  module or  $3 \times 2.5''$  NF/RO module. Sensors are marked as T (temperature), P (pressure transducer), C (EC) and F (flow).

Five types of NF/RO membrane, namely NF270, BW30, NF90, BW30LE and XLE (all sourced from DOW Chemical, USA) were used. NF270 and NF90 are NF membranes while BW30, BW30LE and XLE are brackish water RO membranes. Membrane specifications provided by the manufacturer are summarized in Table 2. It is assumed that the membrane envelopes in both 2.5" and 4" elements have the same dimensions. The difference in their diameters are only due to different numbers of envelopes that are wound into the 2.5" and 4" elements.

Table 2 Membrane specifications as provided by the manufacturer [36-42]

Туре	Active area (m²)	Permeance <sup>a</sup> (L/m <sup>2</sup> .h.bar)	Retention (%)	Maximum feed flow (L/h)	Maximum pressure (bar)	Maximum recovery (%)
4" BW30	7.2	3.4	99.5 <sup>b</sup>	3600	41	90
2.5" BW30	2.6	3.3	99.5 <sup>b</sup>	1400	41	90
4" NF270	7.6	10.8	>97.0°	3600	41	90
2.5" NF270	2.6	10.7	>97.0 <sup>c</sup>	1400	41	90
4" NF90	7.6	8.7	>97.0°	3600	41	90
4" BW30LE	7.6	4.6	99.0 <sup>d</sup>	3600	41	90
2.5" XLE	2.6	7.4	99.0e	1400	41	90

<sup>&</sup>lt;sup>a</sup> Permeance (*P*) was calculate using the equation  $P = \frac{Q_P}{A \times p}$ , where  $Q_P$  was permeate flow at provided test conditions, p is applied pressure and A is membrane active area.

## 2.3. Experimental procedure

In order to have identical solar power quality for all experiments, a solar array simulator (SAS, E4350B, Agilent Technologies, US) was used to power the helical rotor pump (Mono Sun-Sub, Australia). When supplied with solar irradiance data, the SAS functions as a DC power supply that is able to simulate the output of PV modules, thus enabling variable but repeatable solar conditions to be investigated. The simulated PV modules are the ones actually mounted on the PV-membrane

<sup>215</sup> bTest condition: 2000 mg/L NaCl at 15.5 bar, 15% recovery, 25 °C

<sup>&</sup>lt;sup>o</sup> Test condition: 2000 mg/L MgSO4 at 4.8 bar, 15% recovery, 25 °C

d Test condition: 2000 mg/L NaCl at 10.3 bar, 15% recovery, 25 °C

<sup>&</sup>lt;sup>e</sup> Test condition: 500 mg/L NaCl at 6.9 bar, 15% recovery, 25 °C.

system (BP Solar BP3150S, each provide a maximum power of 150 W). A 60-min period of solar irradiance data were recorded in a sunny day during the dry season in Tanzania. The solar irradiance and the resulting motor power of the pump are shown in Figure 2 in the context of the full day of solar irradiance (Figure 2A). The solar irradiance data in Figure 2B are characterized by three features: (i) the maximum intensity of about 1 kW/m², which occurs under cloudless skies; (ii) two short peaks of about 2 min duration occurring at t = 24 and t = 50 min with a minimum solar intensity of 0.36 and 0.19 kW/m², respectively; and (iii) two longer duration peaks (6 to 7 min) at t = 15 and t = 40 with a minimum solar irradiance of 0.35 and 0.18 kW/m², respectively. These dips in solar irradiance occur due to passing clouds. From now on, peaks with 0.35 – 0.36 kW/m² intensity will be referred to as 'light cloud period' and peaks with 0.18 – 0.19 kW/m² intensity as 'heavy cloud period', as indicated in Figure 2. During the period of maximum intensity of solar irradiance (1 kW/m²) the power consumed by the pump was relatively constant at 270 W, which resulted in a constant pressure and feed flow in all experiments.

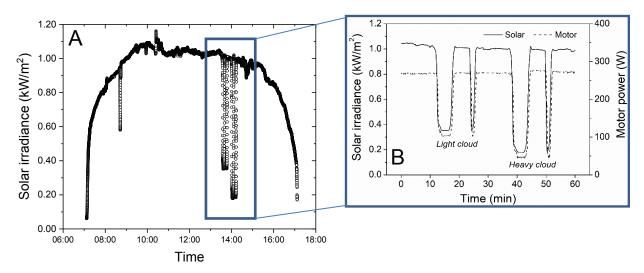


Figure 2 Solar irradiance and the resulting motor power during (A) the full solar day with a controlled fluctuation and (B) the 60-min test period used for the experiments with different membranes and configurations

As there was only one set of sensors in the permeate stream, it was impossible to simultaneously monitor the permeate stream of every element in the  $3 \times 2.5$ " module. Therefore, three repetitive experiments were conducted and in each experiment, one of the three permeate streams was connected to the sensors. Water samples from each permeate stream were manually collected every two minutes for further analyses. Prior to each experiment, the back-pressure valve was adjusted to a point where a similar feed flow was achieved at roughly the same pressure with different modules. The concept of such a "set-point" to enable fair comparison between different system configurations

was discussed in more detail in a previous paper [43]. The set-point for the different modules was chosen to be a pressure of 5.5 – 6.0 bar with a relatively low feed flow of 550 – 600 L/h. The following formulae were used to calculate the parameters to evaluate the performance of the system.

$$R = \left(1 - \frac{C_P}{C_F}\right) \times 100\% \tag{1}$$

$$257 Y = \left(\frac{Q_P}{Q_F}\right) \times 100\% (2)$$

$$\begin{array}{ccc}
J \\
259 & = \frac{Q_P}{A}
\end{array}$$

260 (3)

$$SEC = \frac{I \times U}{Q_P} \tag{4}$$

$$= \frac{Q_{P1}C_{P1} + Q_{P2}C_{P2} + Q_{P3}C_{P3}}{Q_{P1} + Q_{P2} + Q_{P3}}$$
(5)

$$V_{cumulative} = \sum_{i=1}^{t} \left( \frac{Q_{Pi}}{1800} \right) \tag{6}$$

$$C_{cumulative} = \frac{\sum_{j=1}^{t} (C_{Pj} \times V_{j})}{V_{cumulative}}$$

$$(7)$$

In the above equations,  $C_F$  and  $C_P$  are the initial feed and permeate concentration (mg/L), respectively,  $Q_F$  and  $Q_P$  are the feed and permeate flow (L/h), respectively, R is retention (%), Y is recovery (%), J is flux (L/m².h), A is membrane active area (m²), SEC is specific energy consumption (kWh/m³), I is pump current (A), U is pump voltage (V),  $C_{3\times2.5}$  is the fictitious permeate

concentration if three permeate streams of the  $3\times 2.5''$  module were merged (P1, P2, P3 refer to the first, second and third permeate stream, repectively),  $V_{cumulative}$  is the cumulative sum of permeate water volume over time (L),  $C_{cumulative}$  is the cumulative sum of permeate concentration over time (mg/L). For each of the 2.5'' elements, the SEC was calculated using 1/3 of the motor power. To calculate retention for the 2.5'' elements, the original feed concentration, fed to the first element, was considered as feed concentration for all three elements in the  $3\times 2.5''$  module. Pressure drop, expected in the order of 0.03 to 0.15 bar per m (or in this case per element), was not monitored. This pressure drop will be higher for the  $3\times 2.5''$  module due to i) a smaller cross-sectional area and hence higher crossflow velocity, and ii) three modules in series.

## 3. Results & Discussion

## 3.1. Typical system performance over a solar day

To set the work of different module configurations over the 60 min fluctuations period, a typical result over a full day is shown in Figure 3 for the Mdori water and a 1× 4" BW30 module. As the sun rises in the morning (Figure 3A) the motor power (Figure 3B) is determined by the maximum power point tracker and will drive the pump to provide the transmembrane pressure (TMP) (Figure 3C) and feed flow (Figure 3D). This results in a flux (Figure 3E) at a variable recovery and EC retention (Figure 3F). Specific energy consumption (Figure 3G) can be calculated and ultimately the amount of clean water (permeate) produced over such a solar day be determined (Figure 3F). Such data was published previously with very detailed analysis for different waters [10] and for the same water during field work [44] with a focus on transport mechanisms. The retention (in this graph that of EC) varies with fluctuation because diffusion will play a significant role when the applied pressure reduces. The same phenomena is typically observed for EC, IC and F.

Naturally the specific performance will change with membrane type, the main differences will take place during the fluctuation where diffusion contributes disproportionally to permeate quality, while during the maximum solar irradiation the performance of the membrane type can be deducted. For this reason the further investigations are limited to this one hour fluctuation, taking very frequent data readings. This results in a cumulative permeate volume of about 1/10<sup>th</sup> of a full solar day.

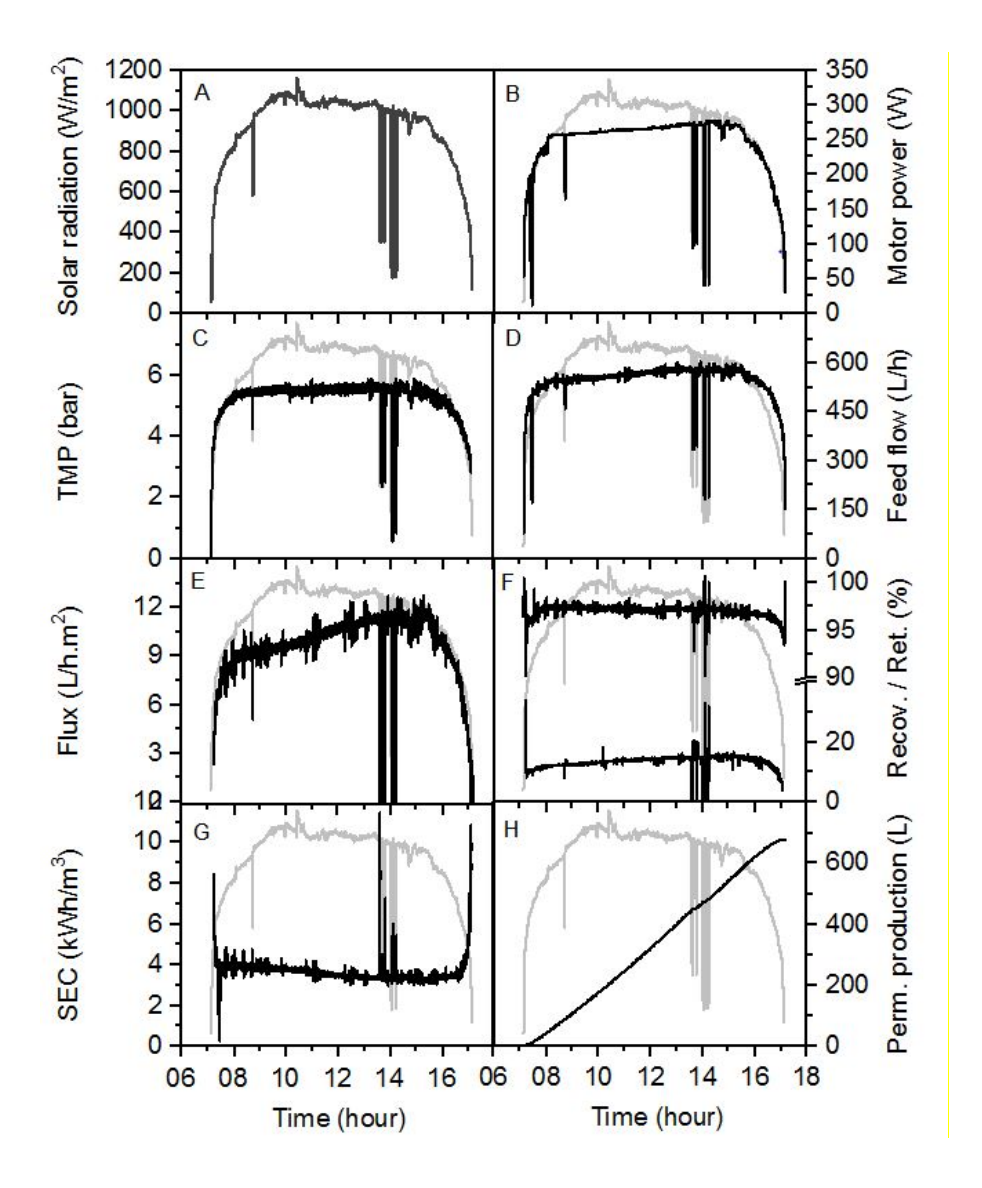


Figure 3 Typical full day experiment with Mdori water and 1×4" module (BW30) with (A) Solar irradiance, (B) motor power, (C) transmembrane pressure (TMP), (D) feed flow, (E) flux, (F) recovery (*bottom*) and retention of electrical conductivity (*top*), (G) specific energy consumption (SEC), and (H) cumulative permeate production.

## 3.2. Performance of the $1 \times 4''$ and $3 \times 2.5''$ modules during cloudless periods

System performance under steady-state conditions was firstly studied as a point of reference for evaluating performance under fluctuating energy. The steady-state region was chosen to be between 34 and 36 min (Figure 2B). The results of NF270 and BW30 membranes in two module sizes (1× 4" and 3× 2.5") are presented in Table 3 and Table 4, respectively. The results of NF90, BW30LE and XLE membranes are presented in the Supplementary Information as Figure S2, S3, and S4, respectively.

Different modules of the same membrane obtained similar pressure and feed flow, confirming that the 'set-point' approach indeed provides a good basis for performance comparison. As shown in

Table 3, the 1× 4" module of NF270 produced permeate at a flux of 35.1 L/m².h and a recovery of 43.9%. The 3× 2.5" module of NF270 had a similar flux of 33.5 L/m² and a recovery of 49.3%. The slightly larger difference in their recoveries was related to their different feed flows. The combined SEC of the 3× 2.5" module was 0.98 kWh/m³, which was identical with that of the 1× 4" module. When it comes to the individual elements, the flux and recovery decreased sharply from the first to the third element. The flux decline was in general caused by a decreased net driving pressure and an increased hydraulic resistance [45, 46]. The decrease of the net driving pressure was the result of (1) the axial pressure drop along the feed channel, and (2) an increase in solute concentration and hence in osmotic pressure due to water permeation and retention [23, 47]. The increased resistance included (1) the friction resistance due to the prolonged flow path and (2) the local resistance when the direction of flow was sharply changed (such as in endcaps and pipe bends) [23, 48, 49]. The SEC increased from the first element to the third element accordingly.

Further, permeate EC, F<sup>-</sup> and IC concentrations from the  $3 \times 2.5''$  and  $1 \times 4''$  modules of NF270 were compared (see Table 3). NF270 is known as a 'loose' NF membrane with a molecular weight cut-off (MWCO) of 155 - 180 Da [31, 50]. NF270 rejects ions mainly based on charge repulsion [31, 51]. The permeate EC and IC of the  $3 \times 2.5''$  module were both lower than that of the  $1 \times 4''$  module. This can be explained by the reduced concentration polarization in the  $3 \times 2.5''$  module. Given that the cross-sectional area of the  $3 \times 2.5''$  module was only one-third of that of the  $1 \times 4''$  module, the crossflow velocity of the  $3 \times 2.5''$  module was approximately triple that of the  $1 \times 4''$  module at the same feed flow. Therefore, the concentration polarization in the  $3 \times 2.5''$  module was more reduced by the higher crossflow velocity [52, 53]. A follow-up study using computational fluid dynamics has revealed that the  $3 \times 2.5''$  module had a lower wall concentration and a smaller boundary layer thickness compared to the  $1 \times 4''$  module [32]. Notably, the permeate F<sup>-</sup> concentration of the  $3 \times 2.5''$  module was higher than those of the  $1 \times 4''$  module. The negative effect of salinity and IC speciation on F<sup>-</sup> retention was attributed to charge screening and Donnan effect [51, 54, 55]. The permeate F<sup>-</sup> concentrations of the  $3 \times 2.5''$  and  $1 \times 4''$  modules were both far beyond the WHO guideline of 1.5 mg/L and this membrane was clearly not suitable to produce potable water.

Within the  $3 \times 2.5''$  module, the permeate concentrations increased sharply from the first element to the third element. The permeate IC and F<sup>-</sup> from the third element were approximately doubled as compared with those from the first element. Such rapid degradation of permeate quality was attributed to: (1) the increased feed concentration from first to third element; and (2) the decreased net driving pressure due to the axial pressure drop and the increased osmotic pressure.

Table 3 Summary of performance indicators of the  $1 \times 4''$  and  $3 \times 2.5''$  modules of NF270 under steady-state operation during cloudless periods (1 kW/m<sup>2</sup> solar irradiance).

	1×4"module	3× 2.5 "module			
		Combined	First element	Second element	Third element
Flux (L/m <sup>2</sup> .h)	35.1	33.5	42.2	30.7	27.7
Recovery (%)	43.9	49.3	20.7	15.0	13.6
SEC (kWh/m³)	0.98	0.98	0.82	1.12	1.25
Permeate EC ( $\mu$ S/cm)	2012.3	1881.5	1554.6	1779.6	2492.3
Permeate F- (mg/L)	25.9	30.2	20.6	30.5	44.4
Permeate IC (mg/L)	176	154	107	154	227

352

353

354

355

356

357

358

359

360

361

362

363

364

365

366

367

368

369

370

371

372

349

350

Not surprisingly, when comparing the performance of BW30 to NF270, the former exhibited a noticeably lower flux and higher SEC, but produced permeate with a higher quality (Table 4). The flux of the  $1 \times 4''$  module of BW30 was 11.7 L/m<sup>2</sup>.h, while the combined permeate flux of the  $3 \times 2.5''$ module was 8.2 L/m<sup>2</sup>.h. The lower flux of the 3× 2.5" module was because of a higher axial pressure drop (a lower net driving pressure) and a higher hydraulic resistance along the feed channel. This is due to the  $3 \times 2.5''$  module being three times as long as the  $1 \times 4''$  module as well as the higher velocity, even though the higher velocity is expected to reduce concentration polarization. Furthermore, the difference in flux between two modules was more significant for BW30 over NF270 due to a higher rejection and hence higher osmotic pressure difference resulting in a lower net driving pressure. Therefore the axial pressure drop probably had a bigger impact on BW30 than on NF270. The SEC of the  $3 \times 2.5''$  module (4.24 kWh/m<sup>3</sup>) was higher than that of the  $1 \times 4''$  module (3.21 kWh/m<sup>3</sup>) as a result of the lower flux. As a 'tight' RO membrane (MWCO 98 Da [50]), BW30 rejects ions primarily based on size exclusion [31]. The permeate EC of the  $3 \times 2.5''$  module was lower than that of the  $1 \times$ 4" module, which suggests that the  $3 \times 2.5$ " module was better than the  $1 \times 4$ " module in rejecting total dissolved salts. However, the permeate F<sup>-</sup> and IC concentrations of the 3× 2.5" module were slightly higher than those of the  $1 \times 4''$  module. A possible explanation is that F<sup>-</sup> and IC (i.e.  $CO_3^{2-}$  and  $HCO_3^{-}$ ) in the 3× 2.5" module were less retained than other larger anions that contributed to EC (such as Cl<sup>-</sup> and SO<sub>4</sub><sup>2-</sup>) by size exclusion [56, 57]. Noticeably, both modules managed to reduce the permeate Fconcentration to meet the WHO guideline of 1.5 mg/L, even for the third element of the 3× 2.5" module.

Table 4 Summary of performance indicators of the  $1 \times 4''$  and  $3 \times 2.5''$  modules of BW30 under steady-state operation during cloudless periods (1 kW/m<sup>2</sup> solar irradiance).

374

375

376

377

378

379

380

381

382

383

384

385

386

387

388

389

390

391

392

393

	1×4"module	3× 2.5 "module			
		Combined	First element	Second element	Third element
Flux (L/m <sup>2</sup> .h)	11.7	8.2	10.9	9.4	4.2
Recovery (%)	14.4	11.4	5.1	4.4	1.9
SEC (kWh/m³)	3.21	4.24	3.17	3.68	8.28
Permeate EC (µS/cm)	134.6	57.5	34.6	63.7	103.5
Permeate F- (mg/L)	0.5	0.8	0.6	0.8	1.2
Permeate IC (mg/L)	3.1	5.4	4.1	5.5	8.5

## 3.3. Performance of the $1 \times 4''$ and $3 \times 2.5''$ modules of NF270 during cloudy periods

The instantaneous performance of the  $1 \times 4''$  and  $3 \times 2.5''$  modules of the loose NF membrane NF270 are presented in Figure 4 and Figure 5, respectively. During the light and heavy cloud periods, the pressure and feed flow decreased sharply due to significant reduction in input power. For the  $1\times$ 4" module, when the solar irradiance dropped from 1 to 0.2 kW/m<sup>2</sup> at 50 min, the pressure reduced from 5.5 to 0.9 bar and the feed flow reduced from 600 to 130 L/h (refer Figure 4A, C). The flux therefore decreased from 35 L/m<sup>2</sup>.h to 0 L/m<sup>2</sup>.h due to insufficient power (see Figure 4E), while the recovery dropped from 44% to 0% accordingly (see Figure 4G). As for the 3× 2.5" module, the variations of pressure and feed flow were very similar to those of the 1× 4" module, except that the feed flow was slightly lower (about 10%) than that of the 1× 4" module (see Figure 4B and D). The lower feed flow of the 3× 2.5" module was probably due to the increased hydraulic resistance. The fluxes – not only the flux from individual element but also the combined flux calculated from total permeate volume and total membrane area – dropped sharply during the light and heavy cloud periods and decreased to 0 L/m<sup>2</sup>.h at 42 and 50 min (Figure 4F). The combined flux of the 3× 2.5" module was equal to the flux of the  $1 \times 4''$  module. The recovery varied with the feed flow and permeate flux (Figure 4H). The combined recovery of the 3× 2.5" module, which equals to the sum of individual recoveries of each element, was slightly higher than the  $1 \times 4''$  module because of its lower feed flow.

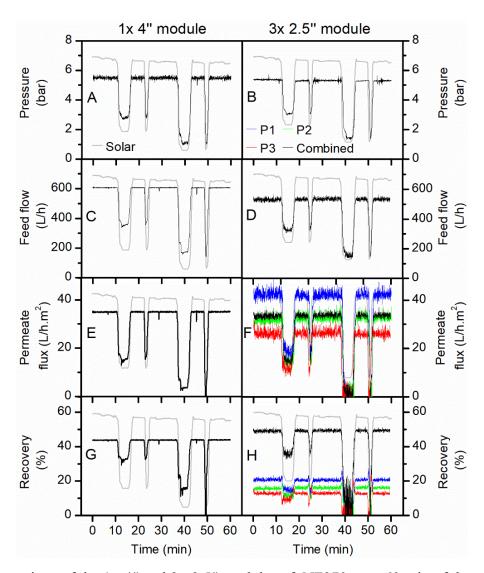


Figure 4 Comparison of the  $1 \times 4''$  and  $3 \times 2.5''$  modules of NF270 over 60 min of the solar day: (A, B) pressure, (C, D) feed flow, (E, F) flux, (G, H) recovery.

Notably, unstable readings were observed in feed flow and flux of the  $3 \times 2.5''$  module. In order to maximize the use of space in the PV-powered membrane system, the three elements in series were arranged vertically from top to bottom. Consequently, the pipes connecting adjacent elements were sharply curved, which caused flow disturbances and thus affected flow measurement [58, 59]. In addition, the tripled length of the flow path, the nearly tripled crossflow velocity, and the excessive number of endcaps in the  $3 \times 2.5''$  module could also contribute to the unstable flow readings. Nevertheless, such unstable readings could be tolerated since they did not shield the measurement under fluctuating solar conditions, which was the specific focus of this study.

The results of the SEC and permeate quality produced by the two modules of NF270 are presented in Figure 5. The SEC mainly depends on the salinity of the water, the permeability of the membrane, the configuration of the system, the recovery, and the efficiency of the pump [60, 61].

There was no markedly difference between the combined SEC of the  $3 \times 2.5''$  module and the SEC of the  $1 \times 4''$  module under maximum intensity of solar irradiance. However, the SEC of the  $3 \times 2.5''$  modules demonstrated more dramatic volatility during the heavy cloud periods, which were attributed to greater variations in the flux values (Figure 5B).

The  $1\times4''$  module showed an increase in EC from 2000 to 3000  $\mu$ S/cm during the light cloud period and from 2000 to 4000  $\mu$ S/cm during the heavy cloud period (Figure 5C). The increased salt concentration during cloudy periods was primarily attributed to the severe drop in flux resulting in less 'dilution'. Besides, the decline in feed flow reduced the crossflow velocity and thus probably facilitated salt diffusion across the membrane [10]. In the  $3\times2.5''$  module, the effect of energy fluctuation on permeate EC was drastic for the third element while the effect was rather moderate for the first two elements. As the available solar irradiance decreased from 1000 to 350 W/m², during the light cloud period, the permeate EC of the first element increased slightly from 1400 to 1800  $\mu$ S/cm, while the third element experienced a drastic increase from 2500 to 4500  $\mu$ S/cm (Figure 5D). During the heavy cloud period, the flux reached 0 L/m².h. The peak appearing at the end of the heavy cloud period was due to the washing away of permeate that remained in the system during this downtime.

The permeate F<sup>-</sup> and IC of both modules varied with solar irradiance in an analogous manner, which exhibited an abrupt peak during the heavy cloud period (Figure 5E–H). This was again because of the severe flux reduction. It is worthwhile mentioning that the permeate F<sup>-</sup> and IC of the third element of the 3× 2.5" module appears to be less affected by energy fluctuation, which seems inconsistent with the trend of the permeate EC. This is in fact due to the two different measurement methods of EC and F<sup>-</sup>/IC, namely in-line monitoring and manual water sampling [62]. The permeate EC was measured continuously by the in-line EC sensor, thereby the EC peaks were precisely recorded. The permeate F<sup>-</sup> and IC concentration, on the other hand, were measured intermittently from discrete samples (samples were taken every two minutes). Inevitably there was some unavoidable error in the peak positions and amplitudes.

Considering the flux, SEC and permeate quality, the performance of the first element of the  $3 \times 2.5''$  module was better than the  $1 \times 4''$  module. However, the deficient performance of the third element of the  $3 \times 2.5''$  module resulted in obtaining a similar overall performance compared to the  $1 \times 4''$  module.

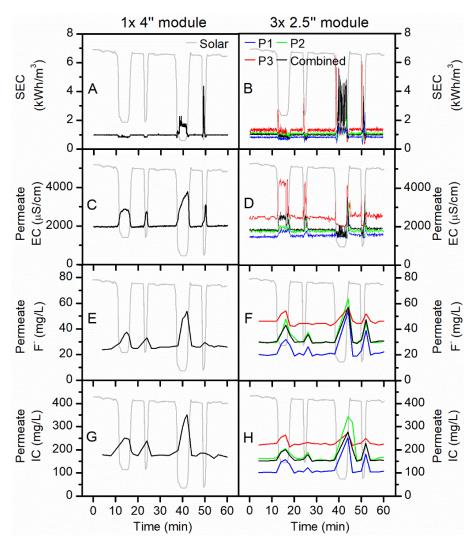


Figure 5 Comparison of the  $1 \times 4''$  and  $3 \times 2.5''$  modules of NF270 over 60 min of the solar day: (A, B) SEC, (C, D) permeate EC, (E, F) permeate F<sup>-</sup> concentration, (G, H) permeate IC concentration.

## 3.4. Performance of the 1×4" and 3×2.5" modules of BW30 during cloudy periods

The effect of changing to a denser SW membrane with high salt retention, BW30, on the performance of the batteryless PV-powered system was studied as well. The results of the performance testing of the two configurations,  $1 \times 4''$  and  $3 \times 2.5''$  BW30 modules, are presented in Figure 6 and Figure 7. The pressure applied to both BW30 module types were nearly identical, as were the feed flows (Figure 6A–D). The unstable readings in feed flow and flux of the  $3 \times 2.5''$  module under steady-state conditions were attributed to flow disturbances, as explained earlier for NF270. Flux and recovery of the  $1 \times 4''$  module of BW30 was notably better than the  $3 \times 2.5''$  module (Figure 6E–H), which was attributed to a lower axial pressure drop and a lower hydraulic resistance. In consequence, the combined SEC of the  $3 \times 2.5''$  module was higher than that of the  $1 \times 4''$  module, let alone the extremely high SEC of the third element of the  $3 \times 2.5''$  module (Figure 7A,B). As discussed

above, the higher rejecting BW30 was more sensitive to axial pressure drop than the NF270 because of a higher osmotic pressure and thus a lower net driving pressure. Therefore the  $3 \times 2.5$ " module performed more poorly compared to the  $1 \times 4$ " module when using BW30.



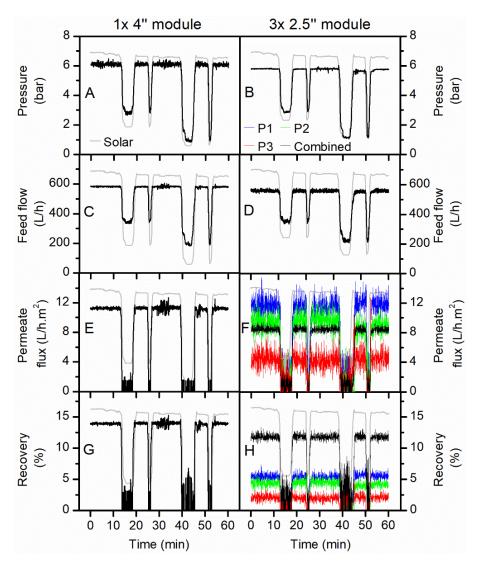


Figure 6 Comparison of the  $1 \times 4''$  and  $3 \times 2.5''$  modules of BW30 over 60 min of the solar day: (A, B) pressure, (C, D) feed flow, (E, F) flux, (G, H) recovery.

It is noteworthy that the flux values of both modules dropped to  $0 \text{ L/m}^2$ .h during the light and heavy cloud periods, which had a negative impact on the permeate quality. There was a spike in the permeate EC upon the end of every cloud period. The zero permeate EC reading during the heavy cloud period was because of air in the sensor (Figure 7C,D). The combined permeate EC of the  $3\times 2.5''$  module was lower than that of the  $1\times 4''$  module, due to the first and third elements of the  $3\times 2.5''$  module exhibiting remarkably efficient salt rejection (Figure 7D). In contrast, the third element

of the  $3 \times 2.5$ " module performed rather poorly in this respect.

Regarding F<sup>-</sup> and IC removal, the performance of 1× 4" module was better than the 3× 2.5" module (Figure 7E–H). When analyzing individual elements of the 3× 2.5" module, the first two elements of the 3× 2.5" module exhibited good removal efficiency while the third element was inefficient in this regard. In fact, the performance of the third element was so poor that it was hardly worth having this element present in the module. It is noteworthy that the permeate F<sup>-</sup> concentration of both modules temporarily exceeded the guideline value during the cloud periods. However, when considering that the permeate was continuously stored in a product tank, the system equipped with BW30 modules was able to produce safe drinking water in a long term, as will be discussed below.

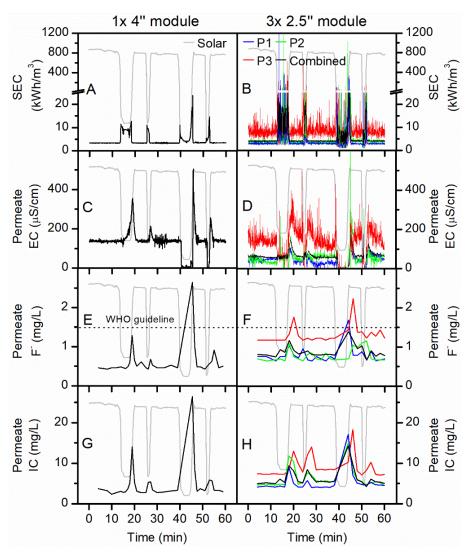


Figure 7 Comparison of the  $1 \times 4''$  and  $3 \times 2.5''$  modules of BW30 over 60 min of the solar day: (A, B) SEC, (C, D) permeate EC, (E, F) permeate F<sup>-</sup> concentration, (G, H) permeate IC concentration.

## 3.5. Overall comparison of the $1 \times 4$ " and $3 \times 2.5$ " modules

As discussed above, the performance of the 1× 4" and 3× 2.5" modules of the NF270 and BW30 membranes were evaluated and compared respectively during both cloudless and cloudy periods. The overall performances of these modules were characterized by two parameters: the first parameter is the cumulative sum of permeate water volume over time, which represents the productivity of the module; the second parameter is the cumulative sum of permeate F<sup>-</sup> concentration over time, which indicates the permeate quality when continuously collected in a tank. The results are shown in Figure 8, along with the results for two other 1× 4" modules (NF90 and BW30LE) and one 3× 2.5" module (XLE), for which the complete performance data are presented in the Supplementary Information. The flux for the first two 2.5" elements is higher (2 mg/L) than that of the 4" element, while permeate F concentration of the 2.5" elements is higher (2 mg/L) than that of the 4" inch element (<1 mg/L). This is somewhat anomalous and because the XLE membrane is not usually included in this research no clear explanation for observation can be provided. Possibly this performance is due to a quality variation between the individual elements.

The cumulative permeate volume of all modules increased linearly with time, apart from during the cloud periods when the productivity was reduced for a short time (Figure 8A). In case of NF270, the permeate volumes produced by both modules were nearly the same (222 – 226 L), whereas for BW30 the  $1\times 4''$  module (63 L) produced a higher permeate volume than the  $3\times 2.5''$  module (52 L). The other three modules contained tight NF (NF90) and low energy RO (BW30LE, XLE) membranes. Their water productivities were around halfway between that of the loose NF (NF270) and the tight RO (BW30) membranes. The overall order was as follows:  $1\times 4''$  NF270 >  $3\times 2.5''$  NF270 >  $1\times 4''$  NF90 >  $3\times 2.5''$  XLE >  $1\times 4''$  BW30LE >  $1\times 4''$  BW30 >  $3\times 2.5''$  BW30, which was completely consistent with the order of the permeance values, as reported in Table 2.

The cumulative permeate F<sup>-</sup> concentration of all modules increased in a stepped manner due to the dramatic soar of transient concentration during the cloud periods (Figure 8B). It is evident that the  $1 \times 4$ " module had a better performance than the  $3 \times 2.5$ " module for both NF270 and BW30. As discussed above, the third element of the  $3 \times 2.5$ " module reduced the overall performance of the module significantly, which was due to the increasing feed concentration and the greater pressure drop along the feed channel. The cumulative permeate F<sup>-</sup> concentration of all modules followed the order:  $3 \times 2.5$ " NF270 >  $1 \times 4$ " NF270 >  $3 \times 2.5$ " XLE >  $1 \times 4$ " NF90 >  $1 \times 4$ " BW30LE >  $3 \times 2.5$ " BW30 >  $1 \times 4$ " BW30. The order of membrane type was in good agreement with the salt rejection data provided by the manufacturer [63]. Even though the cloudy periods did not contribute substantially to water quality in this study, when longer cloud periods are experienced and

consequently the transients are even longer this contribution may need to be controlled to not compromise the overall water quality. Long term tests will be required to evaluate this and the control algorithm and hardware may be expanded to include a permeate flush for such periods.

When refering to the WHO guideline limit for F<sup>-</sup> concentration of 1.5 mg/L, three 1× 4" modules (1× 4" BW30, 1× 4" BW30LE and 1× 4" NF90) and one 3× 2.5" module (3× 2.5" BW30) were able to meet the guideline throughout the 60-min period. The other three modules (3× 2.5" NF270, 1× 4" NF270, and 3× 2.5" XLE), on the contrary, failed to produce permeate with acceptable F<sup>-</sup> concentrations. It should be noted that XLE, as a RO membrane, was designed to have a higher salt rejection than NF90 [63]. The inferior F<sup>-</sup> removal of 3× 2.5" XLE compared to 1× 4" NF90 revealed the significant impact of module size on the actual system performance. The 1× 4" NF90 module seemed to be the best option in balancing permeate productivity and quality, which produced 127 L of drinking water with 1.2 mg/L F<sup>-</sup> within the 60-min period.

When it comes to the cost factor, the market price of three 2.5" elements is much higher than that of one 4" element, let alone the extra associated costs for three elements, such as extra tubing and pressure vessels. It is thus more cost-effective to use the  $1\times 4"$  module rather than the  $3\times 2.5"$  module.

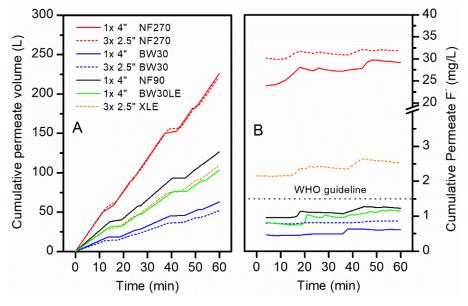


Figure 8 Comparison of cumulative (A) permeate volume and (B) permeate  $F^-$  concentration for different  $1 \times 4''$  and  $3 \times 2.5''$  modules over 60 min of the solar day.

## 4. Conclusions

This study investigated the impact of membrane module size on the performance of a batteryless PV-powered membrane system under fluctuating solar conditions. Several NF/RO

membranes in two module sizes  $(1 \times 4'')$  and  $3 \times 2.5''$ ) of the same membrane area were used to treat a naturally fluoridated brackish water in a remote village in northern Tanzania.

Under steady-state conditions, the  $1\times 4''$  and  $3\times 2.5''$  modules of NF270 achieved good flux  $(33-35 \text{ L/m}^2\text{.h})$  and SEC  $(0.98 \text{ kWh/m}^3)$ , but as expected, the permeate quality  $(25-30 \text{ mg/L F}^-)$  was too poor to meet the drinking water guideline for fluoride. Meanwhile the  $1\times 4''$  and  $3\times 2.5''$  modules of BW30 exhibited much lower flux  $(8-12 \text{ L/m}^2\text{.h})$  and correspondingly a higher SEC  $(3-4 \text{ kWh/m}^3)$ , but the permeate F<sup>-</sup> concentration (0.5-0.8 mg/L) was satisfactory for drinking purposes.

Under fluctuating solar conditions, the pressure and feed flow of the modules decreased drastically, thus reducing the flux and increasing the SEC. The permeate water quality degraded sharply because of the severe drop in flux. The transient permeate F<sup>-</sup> concentration of BW30 modules temporarily exceeded the guideline value. However, if being collected in a product tank, the cumulative permeate F<sup>-</sup> concentration of BW30 could always meet the WHO drinking water guideline. The NF90 and BW30LE modules also achieved very good performance.

The performance of the  $1\times 4''$  module was always equivalent to or better than that of the  $3\times 2.5''$  module of the same membrane. This was mainly because the third element of the  $3\times 2.5''$  module decreased the overall performance of the module substantially. Taking into account the cost factor, large diameter SW modules enable considerable reductions in capital cost and life-cycle cost, thereby increasing the economic feasibility of implementing PV-powered membrane systems in remote and rural locations. Future work will focus on development of appropriate modelling frameworks for performance simulation of PV-powered membrane systems during both steady-state and fluctuating operations.

# 5. Acknowledgements

The research was funded in part by two Leverhulme Royal Society Africa Awards SADWAT-Tanzania and SUCCESS; as well as the Helmholtz Association Recruitment Initiative for AIS and BSR. The Energy Technology Partnership (ETP) and Drinking Water Quality Regulator for Scotland (DWQR) provided the PhD scholarship for JS. The DOW Chemical Company kindly donated the NF/RO membrane modules for this project, and GE Power & Water (Zenon) the UF module. Godfrey Mkongo (Ngurdoto Defluoridation Research Station (NDRS), Tanzania) is greatly appreciated for his hospitality when carrying out experiments at NDRS. William Dahi (Defluoridation Technology Project, Tanzania) carried out the analysis of a huge number of samples, while Elly Karle and Reinhard Sembritzki (KIT, Germany) provided IC and ICP data the source water sample. Minh

- Nguyen (KIT, Germany) is thanked for drawing the graphic of the spiral wound element in the SI.
- Prof Jack Gilron (BGU, Israel) has inspired this work through his questions at the PhD defense of
- 573 Gavin Park.

575

## 6. Supplementary Information

- The SI contains a schematic of a spiral wound module, as well as further data of the NF90,
- 577 BW30LE and XLE membranes.

## **7. References**

- 579 [1] J. Alcamo, N. Fernandez, S.A. Leonard, P. Peduzzi, A. Singh, R. Harding Rohr Reis, 21 issues
- for the 21st Century: results of the UNEP Foresight Process on Emerging Environmental issues,
- 581 (2012).
- 582 [2] B.S. Richards, J. Shen, A.I. Schäfer, Water-energy nexus perspectives in the context of
- 583 photovoltaic-powered decentralized water treatment systems: A Tanzanian case study, Energy
- 584 Technology, (2017) 1-13.
- [3] A.I. Schäfer, A. Broeckmann, B.S. Richards, Renewable Energy Powered Membrane Technology.
- 1. Development and Characterization of a Photovoltaic Hybrid Membrane System, Environmental
- 587 Science & Technology, 41 (2007) 998-1003.
- [4] V.G. Gude, N. Nirmalakhandan, S. Deng, Renewable and sustainable approaches for desalination,
- Renewable and Sustainable Energy Reviews, 14 (2010) 2641-2654.
- 590 [5] M. Shatat, M. Worall, S. Riffat, Opportunities for solar water desalination worldwide: Review,
- 591 Sustainable Cities and Society, 9 (2013) 67-80.
- 592 [6] D. Herold, A. Neskakis, A small PV-driven reverse osmosis desalination plant on the island of
- 593 Gran Canaria, Desalination, 137 (2001) 285-292.
- 594 [7] M. Thomson, D. Infield, A photovoltaic-powered seawater reverse-osmosis system without
- 595 batteries, Desalination, 153 (2003) 1-8.
- [8] A. Chafidz, E.D. Kerme, I. Wazeer, Y. Khalid, A. Ajbar, S.M. Al-Zahrani, Design and fabrication
- of a portable and hybrid solar-powered membrane distillation system, Journal of Cleaner Production,
- 598 133 (2016) 631-647.
- 599 [9] S.M. Shalaby, Reverse osmosis desalination powered by photovoltaic and solar Rankine cycle
- power systems: A review, Renewable and Sustainable Energy Reviews, 73 (2017) 789-797.
- [10] J. Shen, B.S. Richards, A.I. Schäfer, Renewable energy powered membrane technology: Case
- study of St. Dorcas borehole in Tanzania demonstrating fluoride removal via nanofiltration/reverse
- osmosis, Separation and Purification Technology, 170 (2016) 445-452.
- 604 [11] A. Joyce, D. Loureiro, C. Rodrigues, S. Castro, Small reverse osmosis units using PV systems
- for water purification in rural places, Desalination, 137 (2001) 39-44.

- 606 [12] T. Espino, B. Peñate, G. Piernavieja, D. Herold, A. Neskakis, Optimised desalination of seawater
- by a PV powered reverse osmosis plant for a decentralised coastal water supply, Desalination, 156
- 608 (2003) 349-350.
- [13] M.A. Alghoul, P. Poovanaesvaran, M.H. Mohammed, A.M. Fadhil, A.F. Muftah, M.M. Alkilani,
- K. Sopian, Design and experimental performance of brackish water reverse osmosis desalination unit
- powered by 2 kW photovoltaic system, Renewable Energy, 93 (2016) 101-114.
- [14] B.S. Richards, D.P.S. Capão, A.I. Schäfer, Renewable energy powered membrane technology.
- 2. The effect of energy fluctuations on performance of a photovoltaic hybrid membrane system,
- 614 Environmental Science & Technology, 42 (2008) 4563-4569.
- 615 [15] E.S. Mohamed, G. Papadakis, E. Mathioulakis, V. Belessiotis, A direct coupled photovoltaic
- 616 seawater reverse osmosis desalination system toward battery based systems a technical and
- economical experimental comparative study, Desalination, 221 (2008) 17-22.
- [16] M. Thomson, D. Infield, Laboratory demonstration of a photovoltaic-powered seawater reverse-
- osmosis system without batteries, Desalination, 183 (2005) 105-111.
- 620 [17] B.S. Richards, D.P.S. Capão, W.G. Früh, A.I. Schäfer, Renewable energy powered membrane
- 621 technology: Impact of solar irradiance fluctuations on performance of a brackish water reverse
- osmosis system, Separation and Purification Technology, 156, Part 2 (2015) 379-390.
- [18] L.A. Richards, B.S. Richards, A.I. Schäfer, Renewable energy powered membrane technology:
- 624 Salt and inorganic contaminant removal by nanofiltration/reverse osmosis, Journal of Membrane
- 625 Science, 369 (2011) 188-195.
- 626 [19] Dow Water and Process Solutions, FILMTEC<sup>TM</sup> Reverse Osmosis Membranes Technical
- 627 Manual,
- 628 http://msdssearch.dow.com/PublishedLiteratureDOWCOM/dh 095b/0901b8038095b91d.pdf?filepa
- 629 th=/609-00071.pdf&fromPage=GetDoc. Access date: May.
- [20] J. Shen, G. Mkongo, G. Abbt-Braun, S.L. Ceppi, B.S. Richards, A.I. Schäfer, Renewable energy
- powered membrane technology: Fluoride removal in a rural community in northern Tanzania,
- 632 Separation and Purification Technology, 149 (2015) 349-361.
- [21] J. Schwinge, P.R. Neal, D.E. Wiley, D.F. Fletcher, A.G. Fane, Spiral wound modules and spacers:
- Review and analysis, Journal of Membrane Science, 242 (2004) 129-153.
- 635 [22] A.J. Karabelas, M. Kostoglou, C.P. Koutsou, Modeling of spiral wound membrane desalination
- modules and plants review and research priorities, Desalination, 356 (2015) 165-186.
- [23] J. Johnson, M. Busch, Engineering aspects of reverse osmosis module design, Desalination and
- 638 Water Treatment, 15 (2010) 236-248.
- 639 [24] A.J. Karabelas, C.P. Koutsou, M. Kostoglou, The effect of spiral wound membrane element
- design characteristics on its performance in steady state desalination A parametric study,
- 641 Desalination, 332 (2014) 76-90.
- [25] J. Fawell, K. Bailey, J. Chilton, E. Dahi, L. Fewtrell, Y. Magara, Fluoride in drinking water,
- World Health Organization, London 2006.

- [26] J.P. Shorter, J. Massawe, N. Parry, R.W. Walker, Comparison of two village primary schools in
- northern Tanzania affected by fluorosis, International Health, 2 (2010) 269-274.
- 646 [27] H.G. Jarvis, P. Heslop, J. Kisima, W.K. Gray, G. Ndossi, A. Maguire, R.W. Walker, Prevalence
- and aetiology of juvenile skeletal fluorosis in the south-west of the Hai district, Tanzania a
- community-based prevalence and case-control study, Tropical Medicine & International Health, 18
- 649 (2013) 222-229.
- 650 [28] H. Mjengera, G. Mkongo, Appropriate deflouridation technology for use in flourotic areas in
- Tanzania, Physics and Chemistry of the Earth, 28 (2003) 1097-1104.
- [29] S. Ayoob, A.K. Gupta, V.T. Bhat, A conceptual overview on sustainable technologies for the
- defluoridation of drinking water, Critical Reviews in Environmental Science and Technology, 38
- 654 (2008) 401-470.
- [30] K.M.K. Kut, A. Sarswat, A. Srivastava, C.U. Pittman, D. Mohan, A review of fluoride in african
- 656 groundwater and local remediation methods, Groundwater for Sustainable Development, 2-3 (2016)
- 657 190-212.
- 658 [31] J. Shen, A.I. Schäfer, Factors affecting fluoride and natural organic matter (NOM) removal from
- 659 natural waters in Tanzania by nanofiltration/reverse osmosis, Science of The Total Environment,
- 660 527–528 (2015) 520-529.
- 661 [32] C. Onorato, M. Gaedtke, M. Kespe, H. Nirschl, A.I. Schäfer, Renewable energy powered
- membrane technology: computational fluid dynamics evaluation of system performance with variable
- module size and fluctuating energy, Separation and Purification Technology, (2019).
- 664 [33] World Health Organization, Guidelines for drinking-water quality: fourth edition incorporating
- the first addendum, in, Geneva, 2017.
- [34] A.I. Schäfer, A. Broeckmann, B.S. Richards, Renewable energy powered membrane technology.
- 1. development and characterization of a photovoltaic hybrid membrane system, Environmental
- 668 Science & Technology, 41 (2006) 998-1003.
- 669 [35] B.S. Richards, G.L. Park, T. Pietzsch, A.I. Schäfer, Renewable energy powered membrane
- 670 technology: Brackish water desalination system operated using real wind fluctuations and energy
- buffering, Journal of Membrane Science, 468 (2014) 224-232.
- [36] Dow Chemical Company, DOW FILMTEC Fiberglassed Elements for Light Industrial Systems,
- 673 <a href="http://www.dupont.com/content/dam/Dupont2.0/Products/water/literature/609-00350.pdf">http://www.dupont.com/content/dam/Dupont2.0/Products/water/literature/609-00350.pdf</a>. Access
- 674 date: 12 November 2018.
- 675 [37] Dow Chemical Company, FILMTEC Membranes NF270 Nanofiltration Elements for
- 676 Commercial Systems,
- 677 http://www.dupont.com/content/dam/Dupont2.0/Products/water/literature/609-00519.pdf. Access
- 678 date: 12 November 2018.
- 679 [38] Dow Chemical Company, DOW FILMTEC Membranes DOW FILMTEC NF90 Nanofiltration
- 680 Elements for Commercial Systems,
- 681 <a href="http://www.dupont.com/content/dam/Dupont2.0/Products/water/literature/609-00378.pdf">http://www.dupont.com/content/dam/Dupont2.0/Products/water/literature/609-00378.pdf</a>. Access
- 682 date: 12 November 2018.

- [39] Dow Chemical Company, FILMTEC Membranes Basics of RO and NF: Element Characteristics,
- http://msdssearch.dow.com/PublishedLiteratureDOWCOM/dh 0071/0901b803800710df.pdf.
- Access date: 12 November 2018.
- 686 [40] Dow Chemical Company, FILMTEC Membranes System Design: Introduction,
- 687 <a href="http://msdssearch.dow.com/PublishedLiteratureDOWCOM/dh\_0043/0901b803800435bd.pdf?filepa">http://msdssearch.dow.com/PublishedLiteratureDOWCOM/dh\_0043/0901b803800435bd.pdf?filepa</a>
- 688 <u>th=liquidseps/pdfs/noreg/609-02046.pdf.</u> Access date: 12 November 2018.
- 689 [41] Dow Chemical Company, FILMTEC XLE-2540 Membranes Extra Low Energy Elements for
- 690 Commercial Systems,
- 691 <a href="http://www.dupont.com/content/dam/Dupont2.0/Products/water/literature/609-00349.pdf">http://www.dupont.com/content/dam/Dupont2.0/Products/water/literature/609-00349.pdf</a>. Access
- 692 date: 12 November 2018.
- 693 [42] Dow Chemical Company, FILMTEC LE-4040 Membranes Fiberglassed Elements for Light
- Industrial Systems, https://www.lenntech.com/Data-sheets/Dow-Filmtec-LE-4040.pdf. Access date:
- 695 12 November 2018.
- 696 [43] B.S. Richards, G.L. Park, T. Pietzsch, A.I. Schäfer, Renewable energy powered membrane
- 697 technology: Safe operating window of a brackish water desalination system, Journal of Membrane
- 698 Science, 468 (2014) 400-409.
- 699 [44] A.I. Schäfer, J. Shen, B.S. Richards, Renewable energy powered membrane technology:
- Removal of natural organic matter and fluoride in Tanzanian communities, npj Nature Clean Water,
- 701 24 (2018) 1-10.
- 702 [45] A.F. Derradji, S. Taha, G. Dorange, Application of the resistances in series model in
- 703 ultrafiltration, Desalination, 184 (2005) 377-384.
- 704 [46] G. Schock, A. Miguel, Mass transfer and pressure loss in spiral wound modules, Desalination,
- 705 64 (1987) 339-352.
- 706 [47] J. Mulder, Basic Principles of Membrane Technology, Springer, Netherlands, 1996.
- 707 [48] I.E. Idelchik, Handbook of Hydraulic Resistance, Begell House Publishers, USA, 2007.
- 708 [49] MathWorks, Hydraulic resistance in pipe bend,
- 709 https://www.mathworks.com/help/physmod/hydro/ref/pipebend.html. Access date: 12 November
- 710 2018.
- 711 [50] K. Boussu, Y. Zhang, J. Cocquyt, P. Van der Meeren, A. Volodin, C. Van Haesendonck, J.A.
- 712 Martens, B. Van der Bruggen, Characterization of polymeric nanofiltration membranes for systematic
- analysis of membrane performance, Journal of Membrane Science, 278 (2006) 418-427.
- 714 [51] I. Owusu-Agyeman, A. Jeihanipour, T. Luxbacher, A.I. Schäfer, Implications of humic acid,
- 715 inorganic carbon and speciation on fluoride retention mechanisms in nanofiltration and reverse
- osmosis, Journal of Membrane Science, 528 (2017) 82-94.
- 717 [52] H. Choi, K. Zhang, D.D. Dionysiou, D.B. Oerther, G.A. Sorial, Influence of cross-flow velocity
- on membrane performance during filtration of biological suspension, Journal of Membrane Science,
- 719 248 (2005) 189-199.

- 720 [53] J.S. Vrouwenvelder, C. Picioreanu, J.C. Kruithof, M.C.M. van Loosdrecht, Biofouling in spiral
- wound membrane systems: Three-dimensional CFD model based evaluation of experimental data,
- 722 Journal of Membrane Science, 346 (2010) 71-85.
- 723 [54] J. Luo, Y. Wan, Effects of pH and salt on nanofiltration A critical review, Journal of Membrane
- 724 Science, 438 (2013) 18-28.
- 725 [55] S.M.J. Zaidi, F. Fadhillah, Z. Khan, A.F. Ismail, Salt and water transport in reverse osmosis thin
- film composite seawater desalination membranes, Desalination, 368 (2015) 202-213.
- 727 [56] Y. Marcus, Thermodynamics of solvation of ions. Part 5.-Gibbs free energy of hydration at
- 728 298.15 K, Journal of the Chemical Society, Faraday Transactions, 87 (1991) 2995-2999.
- 729 [57] L.A. Richards, B.S. Richards, B. Corry, A.I. Schäfer, Experimental energy barriers to anions
- transporting through nanofiltration membranes, Environmental Science & Technology, 47 (2013)
- 731 1968-1976.
- 732 [58] Seametrics, Resolving flowmeter instability problems, in, USA, 2009.
- 733 [59] G.H. Keulegan, K.H. Beij, Pressure Losses for Fluid Flow in Curved Pipes, US Government
- 734 Printing Office, USA, 1937.
- 735 [60] H.M. Laborde, K.B. França, H. Neff, A.M.N. Lima, Optimization strategy for a small-scale
- reverse osmosis water desalination system based on solar energy, Desalination, 133 (2001) 1-12.
- 737 [61] C. Charcosset, A review of membrane processes and renewable energies for desalination,
- 738 Desalination, 245 (2009) 214-231.
- 739 [62] G.J. Kirmever, Guidance Manual for Monitoring Distribution System Water Quality, American
- 740 Water Works Association, USA, 2002.
- 741 [63] Dow Chemical Company, Dow Water and Process Solutions Levels of Separation of IX, RO,
- NF, UF, https://dowwater.custhelp.com/app/answers/detail/a id/477. Access date: 12 November
- 743 2018.

/46	SUPPLEMENTARY INFURMATION
747	
748	Renewable energy powered membrane technology: experimental
749	investigation of system performance with variable module size and fluctuating
750	energy
751	
752	Junjie Shen <sup>1,2,3</sup> , Azam Jeihanipour <sup>4</sup> , Bryce S. Richards <sup>2,4</sup> , Andrea I. Schäfer <sup>3,5*</sup>
753	
754	<sup>1</sup> Centre for Advanced Separations Engineering, University of Bath, Bath BA2 7AY,
755	United Kingdom
756	<sup>2</sup> School of Engineering and Physical Sciences, Heriot-Watt University, Edinburgh
757	EH14 4AS, United Kingdom
758	<sup>3</sup> Water and Environmental Science and Engineering, Nelson Mandela African Institute of
759	Science and Technology, Arusha, Tanzania
760	<sup>4</sup> Institute of Microstructure Technology (IMT), KIT, Hermann-von-Helmholtz-Platz 1,
761	76344 Eggenstein-Leopoldshafen, Germany
762	<sup>5</sup> Membrane Technology Department, Institute of Functional Interfaces (IFG-MT),
763	Karlsruhe Institute of Technology, Hermann-von-Helmholtz-Platz 1, 76344 Eggenstein-
764	Leopoldshafen, Germany
765	
766	
767	
768	
769	
770	
771	
772	
773	
774	
775	
776	
777	
778	



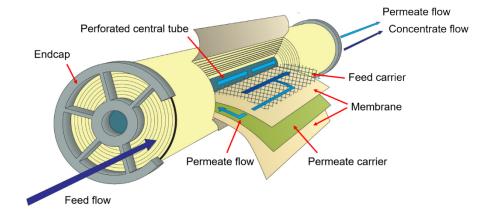


Figure S1 Graphic of a spiral wound element

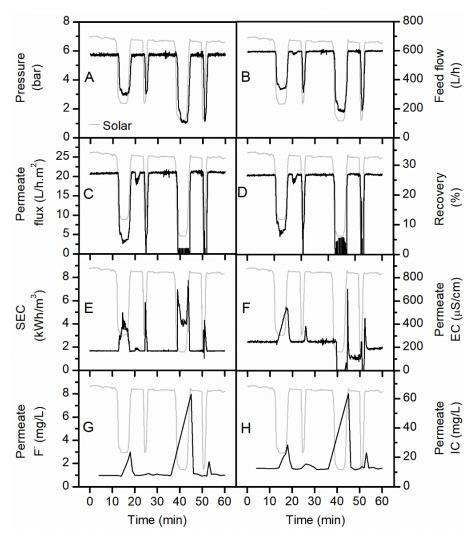


Figure S2 Instantaneous system performance of  $1 \times 4''$  NF90 module over 60 min of the solar day: (A) pressure, (B) feed flow, (C) flux, (D) recovery, (E) SEC, (F) permeate EC, (G) permeate F-concentration, (H) permeate IC concentration

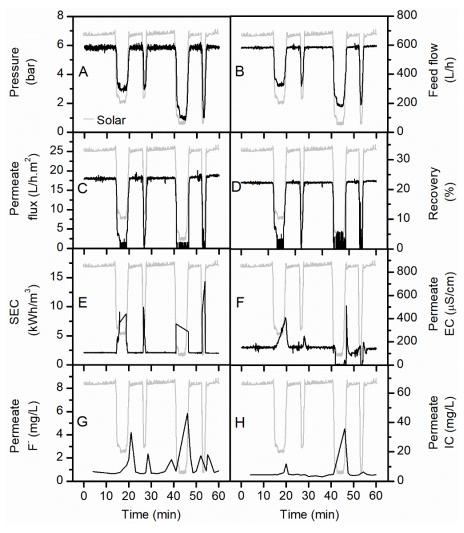


Figure S3 Instantaneous system performance of  $1 \times 4''$  BW30LE module over 60 min of the solar day: (A) pressure, (B) feed flow, (C) flux, (D) recovery, (E) SEC, (F) permeate EC, (G) permeate F<sup>-</sup> concentration, (H) permeate IC concentration

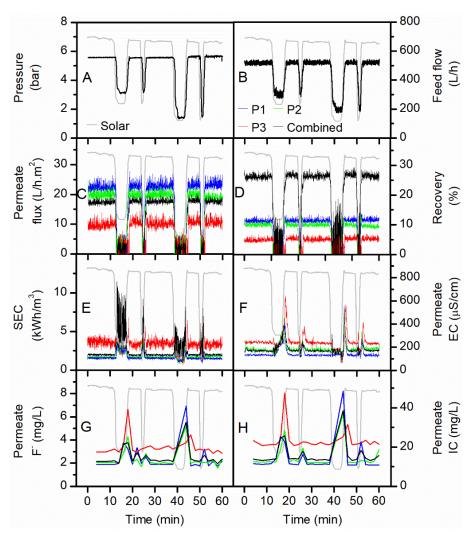
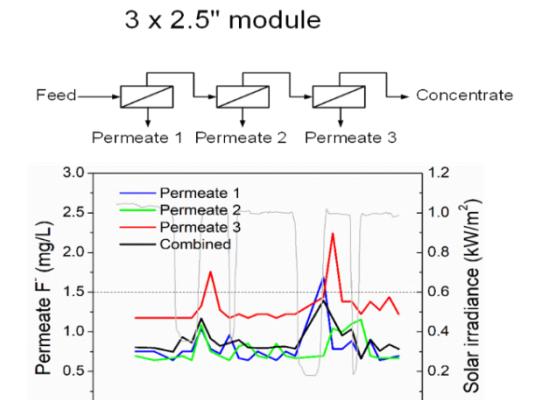


Figure S4 Instantaneous system performance of 3× 2.5" XLE module over 60 min of the solar day: (A) pressure, (B) feed flow, (C) flux, (D) recovery, (E) SEC, (F) permeate EC, (G) permeate F-concentration, (H) permeate IC concentration

# Highlights

- Tanzanian brackish water was treated by a photovoltaic powered NF/RO system
- Two configurations of NF/RO modules with the same membrane area were investigated during a fluctuation period
- The overall performance of the  $1 \times 4''$  module was superior to the  $3 \times 2.5''$  module
- ♦ The third element of the 3× 2.5″ module reduced overall performance significantly
- The cumulative permeate fluoride of BW30, BW30LE and NF90 could meet the guideline

1 x 4" module Concentrate Permeate 3.0 1.2 5.0 9.0 8.0 8.0 Solar irradiance (kW/m²) Permeate F. (mg/L) 2.5 WHO guideline of 1.5 mg/L 0.0 0.0 60 ó 10 20 30 40 50 Time (min)



Time (min)

10 20 30 40 50 60

1	Renewable energy powered membrane technology:						
2	experimental investigation of system performance with						
3	variable module size and fluctuating energy						
4							
5	Junjie Shen <sup>1,2,3</sup> , Azam Jeihanipour⁴, Bryce S. Richards <sup>2,4</sup> , Andrea I. Schäfer <sup>3,5*</sup>						
6							
7	<sup>1</sup> Centre for Advanced Separations Engineering, University of Bath, Bath BA2 7AY,						
8	United Kingdom						
9	<sup>2</sup> School of Engineering and Physical Sciences, Heriot-Watt University, Edinburgh						
10	EH14 4AS, United Kingdom						
11	<sup>3</sup> Water and Environmental Science and Engineering, Nelson Mandela African Institute of Science						
12	and Technology, Arusha, Tanzania						
13	<sup>4</sup> Institute of Microstructure Technology (IMT), KIT, Hermann-von-Helmholtz-Platz 1, 76344						
14	Eggenstein-Leopoldshafen, Germany						
15	<sup>5</sup> Membrane Technology Department, Institute of Functional Interfaces (IFG-MT), Karlsruhe						
16	Institute of Technology, Hermann-von-Helmholtz-Platz 1,						
17	76344 Eggenstein-Leopoldshafen, Germany						
18							
19							
20	Separation and Purification Technology						
21							
22	Submitted 9 April 2018						
23	Resubmitted 12 November 2018 & 2 March 2019						
24							
25							
26							
27							
28							
29							
30							
31							
32	*corresponding author: Prof. Andrea I. Schäfer, +49 (0)721 608 26906						
33	Andrea.Iris.Schaefer@kit.edu						

# Abstract

34

35

36

37

38

39

40

41

42

43

44

45

46

47

48

49

50

51

52

53

Integration of renewable energy and membrane filtration technologies such as nanofiltration (NF) and reverse osmosis (RO) can provide drinking water in places where freshwater is scarce and grid electrical connections are unavailable. This study investigated a directly-connected photovoltaicpowered membrane system under fluctuating solar conditions. Specifically, two configurations of NF/RO membranes with the same membrane area were investigated: a) 1× 4" module, which contained one 4" NF/RO element; and b) 3× 2.5" module, which contained three 2.5" NF/RO elements in series. A high fluoride brackish water ([F-] = 56.2 mg/L, total dissolved solids [TDS] = 4076 mg/L) collected from northern Tanzania was treated by different membranes in the two configurations. Performance indicators such as flux, specific energy consumption, and permeate Fconcentration were monitored over a 60-min period of energy fluctuation that are part of a typical solar day. The results showed that the overall performance of the 1× 4" module was superior to that of the 3× 2.5" module. This is because the performance of a 3× 2.5" module degraded significantly from the first element to the third element due to the increased feed concentration and the decreased net driving pressure. Three 1×4" modules (BW30, BW30LE and NF90) and one 3×2.5" module (BW30) were able to meet the drinking water guideline for fluoride. During cloud periods, the transient permeate F<sup>-</sup> concentration exceeded the guideline value due to insufficient power, however the cumulative permeate F- concentration was always well below the guideline. The photovoltaicpowered membrane system equipped with the above modules provides a promising solution for addressing drinking water problems in remote and rural areas.

54

55

- **Keywords:** brackish water; desalination; module size; fluoride; energy fluctuation; nanofiltration;
- 57 reverse osmosis

5859

# 1. Introduction

The ever-increasing demand for fresh water and clean energy are among the major issues that humans will face and need to solve in the 21st century [1]. The two issues are intertwined via the energy-water nexus, meaning here that drinking water treatment and supply will always require energy [2]. Extreme cases can be found in the many remote locations in both developed and developing countries, which are far away from both centralized water and grid electricity supplies, and where natural freshwater resources are scarce as well [3, 4]. In such cases, the integration of renewable energy (RE) technologies with membrane filtration technologies, namely nanofiltration (NF) and reverse osmosis (RO), provides a sustainable solution for this issue [3-5]. For example, many photovoltaic (PV) powered membrane systems have been successfully implemented throughout the world [6-10]. The figure-of-merit for system performance is typically the specific energy consumption (SEC, units: kWh/m³), which represents how much electricity is required to produce 1 m³ of clean drinking water. The SEC is dependent on feed water salinity, system size, and membrane type [3, 11].

In most PV-powered membrane systems, batteries are used to compensate for variations in solar irradiance [6, 8, 12, 13]. Nevertheless, batteries exhibit several disadvantages such as reducing the overall system efficiency, high capital and maintenance costs, and potential negative environmental impacts in case of improper disposal [7, 14]. Therefore, it has been suggested to avoid the use of batteries in such membrane systems to increase the efficiency and robustness, while decreasing costs [9, 14-16]. However, in such batteryless systems the DC power produced by the PV modules is directly coupled to the pump motor. The system is naturally subjected to widely varying energy availability, which arises from the Earth's rotation, as well as landscape and weather conditions, such as clouds, wind and ambient temperature [17]. The fluctuating current produced by the PV modules subjects the NF/RO membranes integrated into such systems to fluctuations in pressure and flow rate, which affects their flux and permeate water quality [9, 14, 18]. Additionally, manufacturer of NF/RO membranes typically recommend to operate the membrane system in a constant permeate flow rate to increase the life time of the membrane [19]. Richards et al. [18] investigated the effects of fluctuating energy on retention of dissolved contaminants from real water using a PV-powered NF/RO system. It was found that fluctuations in pressure and feed flow, as a result of variation in solar irradiance, impacted the removal of solutes whose retention mechanism was convection/diffusion. However, solutes that were retained via size exclusion and charge repulsion were not affected by fluctuations in solar energy. It has been shown that when a batteryless PVpowered NF/RO system was working under fluctuating conditions, even though the flux was often low, a satisfactory quality of water at a low SEC could be delivered [17, 20]. Further, there is a potential for the NF/RO membrane to possibly benefit from steps in the solar irradiance due to disruption of the concentration polarization layer via a naturally induced backwash occurring when the pump switched off [17].

Currently, spiral wound (SW) modules are the most widely used membrane modules for NF/RO, thanks to their large membrane packing area, high design flexibility, and manufacturability [21]. The construction of a typical SW module can be found in Figure S1. The basic component in a SW module is membrane envelope, which is made of two flat-sheet membranes sealed on three edges, with a permeate carrier filled in between [22, 23]. The achievable performance of a SW module depends not only on the physicochemical characteristics of membrane active surface, but also on the module size parameters, such as membrane envelope number and membrane dimensions [22, 24]. However, there has been little research conducted on the effect of module size on batteryless PVpowered membrane systems. Knowledge of the performance of different module sizes under energyfluctuating conditions is needed for system planning and design, especially for remote and developing areas. It should be noted that during operation with fluctuating energy feed flow and transmembrane pressure vary. This means that pressure drop, concentration polarization (and with this the osmotic pressure at the membrane surface) vary significantly more than in conventionally operated membrane systems. Further, the availability of direct current (DC) equipment such as pumps that are suitable for small systems remains limited. In a scenario where salinity is high, rejection is high and permeability is good and the pressure that can be supplied by the pump is limited, the osmotic pressure may exceed the applied pressure and water permeation is no longer possible. This is typically most likely to happen at the outlet of the module, while during fluctuation this scenario may be more common. In consequence, the design cannot always maintained ideal and studies are aimed at finding the safe operating window (SOW) for a particular water. Remaining within this SOW is a matter of a suitable control system.

This paper addresses this knowledge gap by utilizing two types of SW modules (with comparable membrane areas) in treating a Tanzanian brackish water with high fluoride contents. In Tanzania, excessive fluoride in drinking water has been recognized to cause large-scale health problems, including dental and skeletal fluorosis [25-27]. Current defluoridation methods available in Tanzania, such as adsorption and precipitation, are far from satisfactory due to insufficient removal capacity and complicated maintenance [28-30]. Previous work from has demonstrated that NF/RO membranes are effective in removing fluoride from natural waters in Tanzania [10, 20, 31]. In this study, a batteryless PV-powered membrane system with two types of SW modules will be operated under energy fluctuations. Variations of operating parameters (pressure, feed flow) and performance indicators (flux, SEC, permeate concentration) of the two modules will be compared. In addition, the

performance degradation of each element within the 3× 2.5" module will be investigated. The concentration polarization of such operation was calculated for three energy levels observed from the experimental study using computational fluid dynamics (CFD) for this variable module configuration to understand the transport phenomena [32].

#### 2. Materials and methods

#### 2.1. Water characteristics

A high fluoride content brackish water from a borehole in Mdori, a remote village near Lake Manyara in northern Tanzania (GPS coordinates: S03°47.273′, E035°51.138′), was used as natural water to be treated by NF/RO. 5000 L of water was collected by a water truck on 17 January, 2014. The pH and electrical conductivity (EC) were measured by a pH/conductivity meter (Multi 340i, WTW, Germany). Turbidity was measured using a turbidity meter (TN100, Eutech, Netherlands). Total organic carbon (TOC) and inorganic carbon (IC) were determined by a portable TOC analyzer with autosampler (Sievers 900, GE Analytical Instruments, USA). Fluoride ion (F-) was determined by an ion-selective electrode connected to a pH meter (826 pH Mobile Meter, Metrohm, UK). Chloride (Cl<sup>-</sup>) and sulphate (SO<sub>4</sub><sup>2-</sup>) ions were analyzed by an ion chromatograph (IC 790, Metrohm, Germany). Metal and non-metallic elements were measured via inductively coupled plasma optical emission spectrometry (ICP-OES) (Vista-PRO CCD Simultaneous ICP-OES, Varian, Netherlands). Methods of IC and ICP-OES were described by Shen et al. [20]. Total dissolved solid (TDS) was calculated as the sum of major cations and anions.

The water quality components are presented in Table 1. The water was characterized by high alkalinity (pH 9.7) and high salinity (TDS 4076 mg/L), according to the World Health Organization (WHO) guideline for drinking water [33]. The dominant ions were Na<sup>+</sup>, SO<sub>4</sub><sup>2-</sup>, Cl<sup>-</sup>, and IC, including CO<sub>3</sub><sup>2-</sup> and HCO<sub>3</sub><sup>-</sup>. High levels of salinity and turbidity have no health significance, but they reduce the acceptability of drinking water in terms of its taste, odor and appearance [33]. The F<sup>-</sup> concentration was 56.2 mg/L, which exceeded the WHO guideline of 1.5 mg/L by more than 37 times. Such high level of F<sup>-</sup> poses a genuine health risk of dental and skeletal fluorosis [25]. Therefore, F<sup>-</sup>, IC and EC (represents salinity) were the three target components to treat in order to produce acceptable drinking water from the Mdori brackish water.

163

164

165

166

167

168

169

170

171

172

173

174

175

Table 1 Water quality at Mdori borehole in northern Tanzania (GPS coordinates: S03°47.273', E035°51.138'), compared to WHO guidelines

Parameter Unit		Value	WHO guideline [33]	
pH (25 °C)	_	9.7	6.5-8.5	
EC (25 °C)	μS/cm	4940	_	
TDS	mg/L	$4076^{a}$	1000 <sup>b</sup>	
Turbidity	NTU	15.8	1°	
TOC	mg/L	5.3	_	
IC	mg/L	430.0	_	
F-	mg/L	56.2	1.5	
Cl-	mg/L	268.0	250 <sup>b</sup>	
SO <sub>4</sub> <sup>2-</sup>	mg/L	306.1	250 <sup>b</sup>	
Al	mg/L	0.1	$0.1^d$	
В	mg/L	1.9	2.4	
Ca	mg/L	1.6	$300^{b}$	
Fe	mg/L	0.2	$0.3^{\mathrm{b}}$	
K	mg/L	16.3	_	
Mg	mg/L	0.5	_	
Na	mg/L	1358.1	$200^{\mathrm{b}}$	
P	mg/L	0.7	_	
Si	mg/L	17.3	_	
Sr	mg/L	0.1	_	

<sup>&</sup>lt;sup>a</sup> Calculated as the sum of cations and anions, the charge difference between cations and anions < 5%.

#### *2.2.* System design and membrane characteristics

An integrated PV-powered membrane system was used for the experiments. The filtration system combines ultrafiltration (UF) and NF/RO processes. The UF stage was used to remove particles, viruses and bacteria while the NF/RO stage was for desalination. A schematic is shown in Figure 1, while full details of the system have been published elsewhere [20, 34, 35]. As part of the design concept this system includes some unusual features; the system is operated at relatively low recovery (10-30%) and there is no energy recovery in the system (in form of a booster pump) that would enhance this recovery. The reason is firstly that very few suitable DC components exist to allow such operation for non-seawater systems. Secondly, provided the water is of such quality that

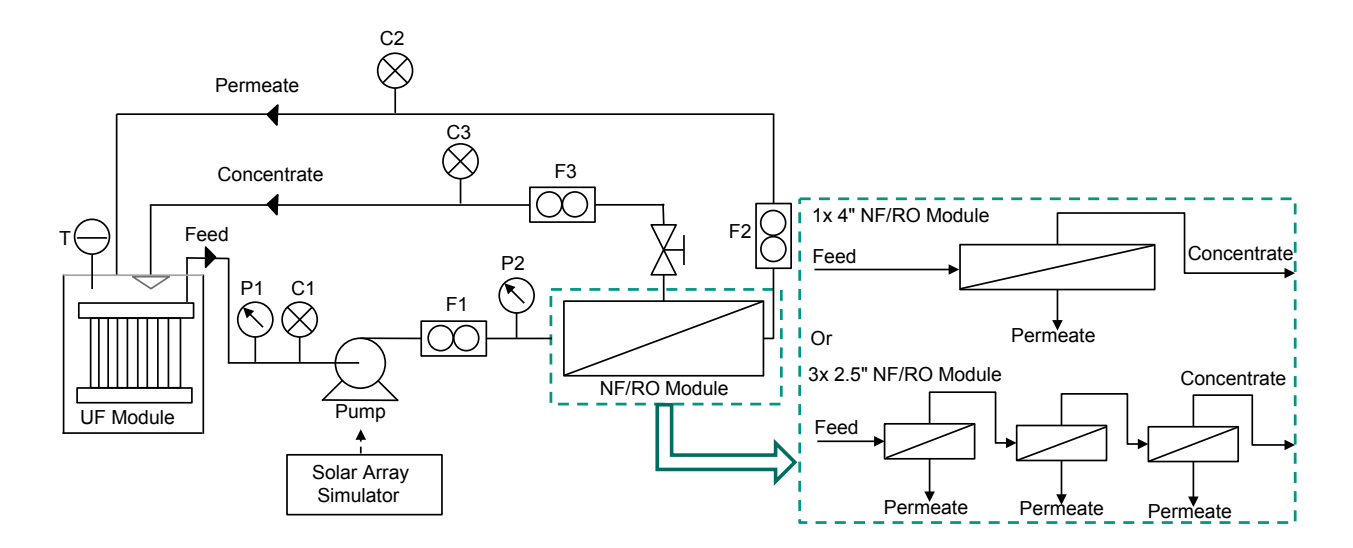
<sup>&</sup>lt;sup>b</sup>Based on average taste thresholds.

<sup>&</sup>lt;sup>c</sup> Based on disinfection effectiveness.

<sup>&</sup>lt;sup>d</sup> Based on optimization of the coagulation process.

after the physical disinfection stage (UF) it can be safely used for washing or showering purposes, then this approach allows to avoid concentrate production. This is highly beneficial in remote areas where no adequate treatment of such concentrates is feasible. In this case this is indeed possible, as the feed water was used for laundry where fluoride is not a concern and the marginal increase in salinity can be tolerated.

The NF/RO elements were spiral wound in 40" (1 m) length and in two different diameters, 2.5" and 4". Two different configurations, or modules, of the NF/RO elements were tested. The first module contained one 4" NF/RO element (denoted as the 1× 4" module), and the second module contained three 2.5" elements in series (denoted as the 3× 2.5" module) such that the concentrate of the first element became the feed to the second, and the concentrate of the second the feed of the third. Therefore, the length of the  $3 \times 2.5''$  module was triple the length of the  $1 \times 4''$  module, while the cross-sectional area of the  $3 \times 2.5$ " module was approximately one-third of that of the  $1 \times 4$ " module. In the 1× 4" module, the permeate and concentrate streams were recirculated into the feed tank; in the 3× 2.5" module, the three permeate streams (one from each element) and the concentrate stream of the last element were recirculated to the feed tank, separately. Pressure, temperature, flow rate and EC sensors were installed on the feed, permeate and concentrate streams. The sensor details can be found in a previous publication [35]. As the system was adapted to install the  $3 \times 2.5$ " module in the existing system, no additional pressure sensors were added and hence the pressure drop across the individual modules is not available. This was exacerbated by the concentrate pressure sensor being not fully functional. These are a design and operational shortfalls that could not be remedied during the field work. Data from the sensors were recorded by a datalogger at 2 second intervals and transferred to a laptop using LabVIEW 8.0 software.



176

177

178

179

180

181

182

183

184

185

186

187

188

189

190

191

192

193

194

195

196

197

Figure 1 Schematic of the PV-powered membrane system configurations equipped with either  $1 \times 4''$  module or  $3 \times 2.5''$  NF/RO module. Sensors are marked as T (temperature), P (pressure transducer), C (EC) and F (flow).

Five types of NF/RO membrane, namely NF270, BW30, NF90, BW30LE and XLE (all sourced from DOW Chemical, USA) were used. NF270 and NF90 are NF membranes while BW30, BW30LE and XLE are brackish water RO membranes. Membrane specifications provided by the manufacturer are summarized in Table 2. It is assumed that the membrane envelopes in both 2.5" and 4" elements have the same dimensions. The difference in their diameters are only due to different numbers of envelopes that are wound into the 2.5" and 4" elements.

Table 2 Membrane specifications as provided by the manufacturer [36-42]

Туре	Active area (m²)	Permeance <sup>a</sup> (L/m <sup>2</sup> .h.bar)	Retention (%)	Maximum feed flow (L/h)	Maximum pressure (bar)	Maximum recovery (%)
4" BW30	7.2	3.4	99.5 <sup>b</sup>	3600	41	90
2.5" BW30	2.6	3.3	99.5 <sup>b</sup>	1400	41	90
4" NF270	7.6	10.8	>97.0°	3600	41	90
2.5" NF270	2.6	10.7	>97.0 <sup>c</sup>	1400	41	90
4" NF90	7.6	8.7	>97.0°	3600	41	90
4" BW30LE	7.6	4.6	99.0 <sup>d</sup>	3600	41	90
2.5" XLE	2.6	7.4	99.0e	1400	41	90

<sup>&</sup>lt;sup>a</sup> Permeance (*P*) was calculate using the equation  $P = \frac{Q_P}{A \times p}$ , where  $Q_P$  was permeate flow at provided test conditions, p is applied pressure and A is membrane active area.

#### 2.3. Experimental procedure

In order to have identical solar power quality for all experiments, a solar array simulator (SAS, E4350B, Agilent Technologies, US) was used to power the helical rotor pump (Mono Sun-Sub, Australia). When supplied with solar irradiance data, the SAS functions as a DC power supply that is able to simulate the output of PV modules, thus enabling variable but repeatable solar conditions to be investigated. The simulated PV modules are the ones actually mounted on the PV-membrane

<sup>215</sup> bTest condition: 2000 mg/L NaCl at 15.5 bar, 15% recovery, 25 °C

<sup>&</sup>lt;sup>o</sup> Test condition: 2000 mg/L MgSO4 at 4.8 bar, 15% recovery, 25 °C

d Test condition: 2000 mg/L NaCl at 10.3 bar, 15% recovery, 25 °C

<sup>&</sup>lt;sup>e</sup> Test condition: 500 mg/L NaCl at 6.9 bar, 15% recovery, 25 °C.

system (BP Solar BP3150S, each provide a maximum power of 150 W). A 60-min period of solar irradiance data were recorded in a sunny day during the dry season in Tanzania. The solar irradiance and the resulting motor power of the pump are shown in Figure 2 in the context of the full day of solar irradiance (Figure 2A). The solar irradiance data in Figure 2B are characterized by three features: (i) the maximum intensity of about 1 kW/m², which occurs under cloudless skies; (ii) two short peaks of about 2 min duration occurring at t = 24 and t = 50 min with a minimum solar intensity of 0.36 and 0.19 kW/m², respectively; and (iii) two longer duration peaks (6 to 7 min) at t = 15 and t = 40 with a minimum solar irradiance of 0.35 and 0.18 kW/m², respectively. These dips in solar irradiance occur due to passing clouds. From now on, peaks with 0.35 – 0.36 kW/m² intensity will be referred to as 'light cloud period' and peaks with 0.18 – 0.19 kW/m² intensity as 'heavy cloud period', as indicated in Figure 2. During the period of maximum intensity of solar irradiance (1 kW/m²) the power consumed by the pump was relatively constant at 270 W, which resulted in a constant pressure and feed flow in all experiments.

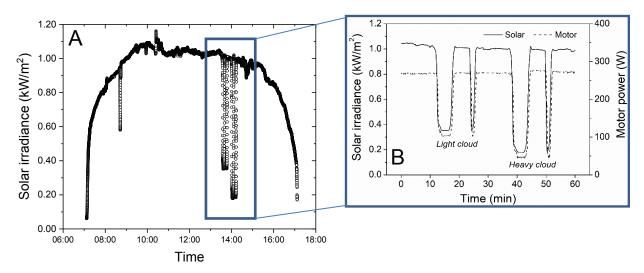


Figure 2 Solar irradiance and the resulting motor power during (A) the full solar day with a controlled fluctuation and (B) the 60-min test period used for the experiments with different membranes and configurations

As there was only one set of sensors in the permeate stream, it was impossible to simultaneously monitor the permeate stream of every element in the  $3 \times 2.5$ " module. Therefore, three repetitive experiments were conducted and in each experiment, one of the three permeate streams was connected to the sensors. Water samples from each permeate stream were manually collected every two minutes for further analyses. Prior to each experiment, the back-pressure valve was adjusted to a point where a similar feed flow was achieved at roughly the same pressure with different modules. The concept of such a "set-point" to enable fair comparison between different system configurations

was discussed in more detail in a previous paper [43]. The set-point for the different modules was chosen to be a pressure of 5.5 – 6.0 bar with a relatively low feed flow of 550 – 600 L/h. The following formulae were used to calculate the parameters to evaluate the performance of the system.

$$R = \left(1 - \frac{C_P}{C_F}\right) \times 100\% \tag{1}$$

$$257 Y = \left(\frac{Q_P}{Q_F}\right) \times 100\% (2)$$

$$\begin{array}{ccc}
J \\
259 & = \frac{Q_P}{A}
\end{array}$$

260 (3)

$$SEC = \frac{I \times U}{Q_P} \tag{4}$$

$$= \frac{Q_{P1}C_{P1} + Q_{P2}C_{P2} + Q_{P3}C_{P3}}{Q_{P1} + Q_{P2} + Q_{P3}}$$
(5)

$$V_{cumulative} = \sum_{i=1}^{t} \left( \frac{Q_{Pi}}{1800} \right) \tag{6}$$

$$C_{cumulative} = \frac{\sum_{j=1}^{t} (C_{Pj} \times V_{j})}{V_{cumulative}}$$

$$(7)$$

In the above equations,  $C_F$  and  $C_P$  are the initial feed and permeate concentration (mg/L), respectively,  $Q_F$  and  $Q_P$  are the feed and permeate flow (L/h), respectively, R is retention (%), Y is recovery (%), J is flux (L/m².h), A is membrane active area (m²), SEC is specific energy consumption (kWh/m³), I is pump current (A), U is pump voltage (V),  $C_{3\times2.5}$  is the fictitious permeate

concentration if three permeate streams of the  $3\times 2.5''$  module were merged (P1, P2, P3 refer to the first, second and third permeate stream, repectively),  $V_{cumulative}$  is the cumulative sum of permeate water volume over time (L),  $C_{cumulative}$  is the cumulative sum of permeate concentration over time (mg/L). For each of the 2.5'' elements, the SEC was calculated using 1/3 of the motor power. To calculate retention for the 2.5'' elements, the original feed concentration, fed to the first element, was considered as feed concentration for all three elements in the  $3\times 2.5''$  module. Pressure drop, expected in the order of 0.03 to 0.15 bar per m (or in this case per element), was not monitored. This pressure drop will be higher for the  $3\times 2.5''$  module due to i) a smaller cross-sectional area and hence higher crossflow velocity, and ii) three modules in series.

# 3. Results & Discussion

### 3.1. Typical system performance over a solar day

To set the work of different module configurations over the 60 min fluctuations period, a typical result over a full day is shown in Figure 3 for the Mdori water and a 1× 4" BW30 module. As the sun rises in the morning (Figure 3A) the motor power (Figure 3B) is determined by the maximum power point tracker and will drive the pump to provide the transmembrane pressure (TMP) (Figure 3C) and feed flow (Figure 3D). This results in a flux (Figure 3E) at a variable recovery and EC retention (Figure 3F). Specific energy consumption (Figure 3G) can be calculated and ultimately the amount of clean water (permeate) produced over such a solar day be determined (Figure 3F). Such data was published previously with very detailed analysis for different waters [10] and for the same water during field work [44] with a focus on transport mechanisms. The retention (in this graph that of EC) varies with fluctuation because diffusion will play a significant role when the applied pressure reduces. The same phenomena is typically observed for EC, IC and F.

Naturally the specific performance will change with membrane type, the main differences will take place during the fluctuation where diffusion contributes disproportionally to permeate quality, while during the maximum solar irradiation the performance of the membrane type can be deducted. For this reason the further investigations are limited to this one hour fluctuation, taking very frequent data readings. This results in a cumulative permeate volume of about 1/10<sup>th</sup> of a full solar day.

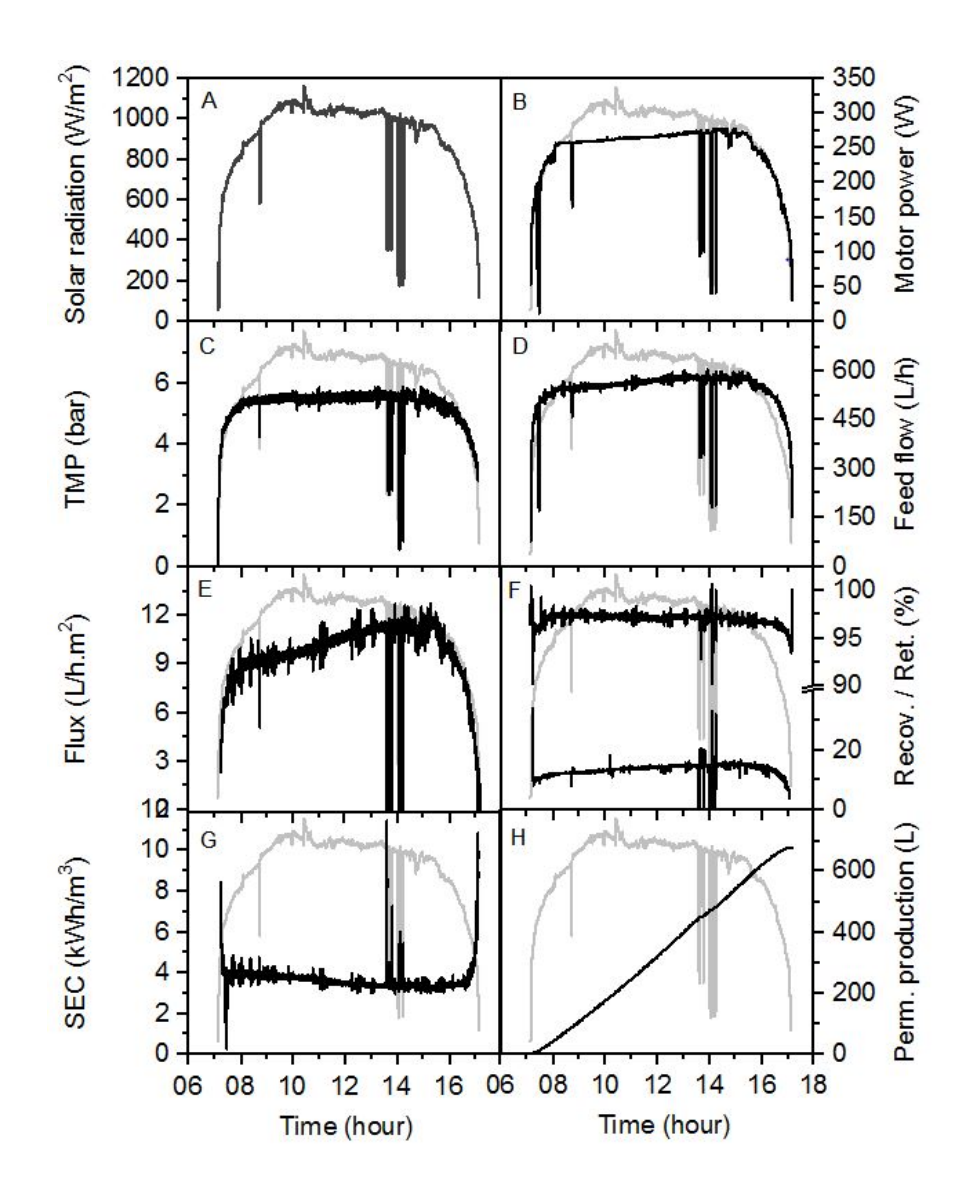


Figure 3 Typical full day experiment with Mdori water and 1×4" module (BW30) with (A) Solar irradiance, (B) motor power, (C) transmembrane pressure (TMP), (D) feed flow, (E) flux, (F) recovery (*bottom*) and retention of electrical conductivity (*top*), (G) specific energy consumption (SEC), and (H) cumulative permeate production.

#### 3.2. Performance of the $1 \times 4$ " and $3 \times 2.5$ " modules during cloudless periods

System performance under steady-state conditions was firstly studied as a point of reference for evaluating performance under fluctuating energy. The steady-state region was chosen to be between 34 and 36 min (Figure 2B). The results of NF270 and BW30 membranes in two module sizes (1× 4" and 3× 2.5") are presented in Table 3 and Table 4, respectively. The results of NF90, BW30LE and XLE membranes are presented in the Supplementary Information as Figure S2, S3, and S4, respectively.

Different modules of the same membrane obtained similar pressure and feed flow, confirming that the 'set-point' approach indeed provides a good basis for performance comparison. As shown in

Table 3, the 1× 4" module of NF270 produced permeate at a flux of 35.1 L/m².h and a recovery of 43.9%. The 3× 2.5" module of NF270 had a similar flux of 33.5 L/m² and a recovery of 49.3%. The slightly larger difference in their recoveries was related to their different feed flows. The combined SEC of the 3× 2.5" module was 0.98 kWh/m³, which was identical with that of the 1× 4" module. When it comes to the individual elements, the flux and recovery decreased sharply from the first to the third element. The flux decline was in general caused by a decreased net driving pressure and an increased hydraulic resistance [45, 46]. The decrease of the net driving pressure was the result of (1) the axial pressure drop along the feed channel, and (2) an increase in solute concentration and hence in osmotic pressure due to water permeation and retention [23, 47]. The increased resistance included (1) the friction resistance due to the prolonged flow path and (2) the local resistance when the direction of flow was sharply changed (such as in endcaps and pipe bends) [23, 48, 49]. The SEC increased from the first element to the third element accordingly.

Further, permeate EC, F<sup>-</sup> and IC concentrations from the  $3 \times 2.5''$  and  $1 \times 4''$  modules of NF270 were compared (see Table 3). NF270 is known as a 'loose' NF membrane with a molecular weight cut-off (MWCO) of 155 - 180 Da [31, 50]. NF270 rejects ions mainly based on charge repulsion [31, 51]. The permeate EC and IC of the  $3 \times 2.5''$  module were both lower than that of the  $1 \times 4''$  module. This can be explained by the reduced concentration polarization in the  $3 \times 2.5''$  module. Given that the cross-sectional area of the  $3 \times 2.5''$  module was only one-third of that of the  $1 \times 4''$  module, the crossflow velocity of the  $3 \times 2.5''$  module was approximately triple that of the  $1 \times 4''$  module at the same feed flow. Therefore, the concentration polarization in the  $3 \times 2.5''$  module was more reduced by the higher crossflow velocity [52, 53]. A follow-up study using computational fluid dynamics has revealed that the  $3 \times 2.5''$  module had a lower wall concentration and a smaller boundary layer thickness compared to the  $1 \times 4''$  module [32]. Notably, the permeate F<sup>-</sup> concentration of the  $3 \times 2.5''$  module was higher than those of the  $1 \times 4''$  module. The negative effect of salinity and IC speciation on F<sup>-</sup> retention was attributed to charge screening and Donnan effect [51, 54, 55]. The permeate F<sup>-</sup> concentrations of the  $3 \times 2.5''$  and  $1 \times 4''$  modules were both far beyond the WHO guideline of 1.5 mg/L and this membrane was clearly not suitable to produce potable water.

Within the  $3 \times 2.5''$  module, the permeate concentrations increased sharply from the first element to the third element. The permeate IC and F<sup>-</sup> from the third element were approximately doubled as compared with those from the first element. Such rapid degradation of permeate quality was attributed to: (1) the increased feed concentration from first to third element; and (2) the decreased net driving pressure due to the axial pressure drop and the increased osmotic pressure.

Table 3 Summary of performance indicators of the  $1 \times 4''$  and  $3 \times 2.5''$  modules of NF270 under steady-state operation during cloudless periods (1 kW/m<sup>2</sup> solar irradiance).

	1×4"module	3× 2.5 ″module			
		Combined	First element	Second element	Third element
Flux (L/m <sup>2</sup> .h)	35.1	33.5	42.2	30.7	27.7
Recovery (%)	43.9	49.3	20.7	15.0	13.6
SEC (kWh/m³)	0.98	0.98	0.82	1.12	1.25
Permeate EC ( $\mu$ S/cm)	2012.3	1881.5	1554.6	1779.6	2492.3
Permeate F- (mg/L)	25.9	30.2	20.6	30.5	44.4
Permeate IC (mg/L)	176	154	107	154	227

352

353

354

355

356

357

358

359

360

361

362

363

364

365

366

367

368

369

370

371

372

349

350

Not surprisingly, when comparing the performance of BW30 to NF270, the former exhibited a noticeably lower flux and higher SEC, but produced permeate with a higher quality (Table 4). The flux of the  $1 \times 4''$  module of BW30 was 11.7 L/m<sup>2</sup>.h, while the combined permeate flux of the  $3 \times 2.5''$ module was 8.2 L/m<sup>2</sup>.h. The lower flux of the 3× 2.5" module was because of a higher axial pressure drop (a lower net driving pressure) and a higher hydraulic resistance along the feed channel. This is due to the  $3 \times 2.5''$  module being three times as long as the  $1 \times 4''$  module as well as the higher velocity, even though the higher velocity is expected to reduce concentration polarization. Furthermore, the difference in flux between two modules was more significant for BW30 over NF270 due to a higher rejection and hence higher osmotic pressure difference resulting in a lower net driving pressure. Therefore the axial pressure drop probably had a bigger impact on BW30 than on NF270. The SEC of the  $3 \times 2.5''$  module (4.24 kWh/m<sup>3</sup>) was higher than that of the  $1 \times 4''$  module (3.21 kWh/m<sup>3</sup>) as a result of the lower flux. As a 'tight' RO membrane (MWCO 98 Da [50]), BW30 rejects ions primarily based on size exclusion [31]. The permeate EC of the  $3 \times 2.5''$  module was lower than that of the  $1 \times$ 4" module, which suggests that the  $3 \times 2.5$ " module was better than the  $1 \times 4$ " module in rejecting total dissolved salts. However, the permeate F<sup>-</sup> and IC concentrations of the 3× 2.5" module were slightly higher than those of the  $1 \times 4''$  module. A possible explanation is that F<sup>-</sup> and IC (i.e.  $CO_3^{2-}$  and  $HCO_3^{-}$ ) in the 3× 2.5" module were less retained than other larger anions that contributed to EC (such as Cl<sup>-</sup> and SO<sub>4</sub><sup>2-</sup>) by size exclusion [56, 57]. Noticeably, both modules managed to reduce the permeate Fconcentration to meet the WHO guideline of 1.5 mg/L, even for the third element of the 3× 2.5" module.

Table 4 Summary of performance indicators of the  $1 \times 4''$  and  $3 \times 2.5''$  modules of BW30 under steady-state operation during cloudless periods (1 kW/m<sup>2</sup> solar irradiance).

374

375

376

377

378

379

380

381

382

383

384

385

386

387

388

389

390

391

392

393

	1× 4 "module	3× 2.5 "module			
		Combined	First element	Second element	Third element
Flux (L/m <sup>2</sup> .h)	11.7	8.2	10.9	9.4	4.2
Recovery (%)	14.4	11.4	5.1	4.4	1.9
SEC (kWh/m³)	3.21	4.24	3.17	3.68	8.28
Permeate EC (µS/cm)	134.6	57.5	34.6	63.7	103.5
Permeate F- (mg/L)	0.5	0.8	0.6	0.8	1.2
Permeate IC (mg/L)	3.1	5.4	4.1	5.5	8.5

# 3.3. Performance of the $1 \times 4''$ and $3 \times 2.5''$ modules of NF270 during cloudy periods

The instantaneous performance of the  $1 \times 4''$  and  $3 \times 2.5''$  modules of the loose NF membrane NF270 are presented in Figure 4 and Figure 5, respectively. During the light and heavy cloud periods, the pressure and feed flow decreased sharply due to significant reduction in input power. For the  $1\times$ 4" module, when the solar irradiance dropped from 1 to 0.2 kW/m<sup>2</sup> at 50 min, the pressure reduced from 5.5 to 0.9 bar and the feed flow reduced from 600 to 130 L/h (refer Figure 4A, C). The flux therefore decreased from 35 L/m<sup>2</sup>.h to 0 L/m<sup>2</sup>.h due to insufficient power (see Figure 4E), while the recovery dropped from 44% to 0% accordingly (see Figure 4G). As for the 3× 2.5" module, the variations of pressure and feed flow were very similar to those of the 1× 4" module, except that the feed flow was slightly lower (about 10%) than that of the 1× 4" module (see Figure 4B and D). The lower feed flow of the 3× 2.5" module was probably due to the increased hydraulic resistance. The fluxes – not only the flux from individual element but also the combined flux calculated from total permeate volume and total membrane area – dropped sharply during the light and heavy cloud periods and decreased to 0 L/m<sup>2</sup>.h at 42 and 50 min (Figure 4F). The combined flux of the 3× 2.5" module was equal to the flux of the  $1 \times 4''$  module. The recovery varied with the feed flow and permeate flux (Figure 4H). The combined recovery of the 3× 2.5" module, which equals to the sum of individual recoveries of each element, was slightly higher than the  $1 \times 4''$  module because of its lower feed flow.

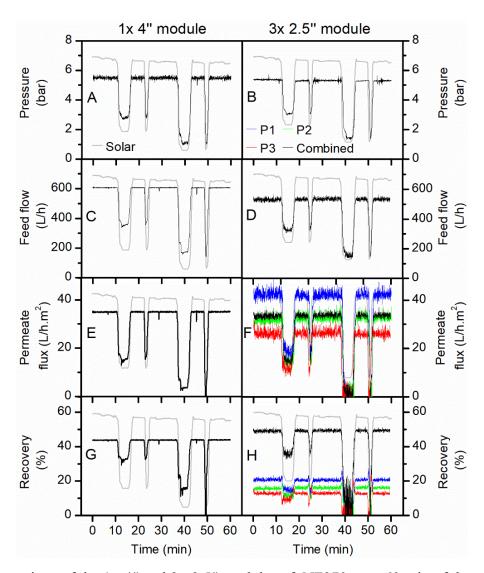


Figure 4 Comparison of the  $1 \times 4''$  and  $3 \times 2.5''$  modules of NF270 over 60 min of the solar day: (A, B) pressure, (C, D) feed flow, (E, F) flux, (G, H) recovery.

Notably, unstable readings were observed in feed flow and flux of the  $3 \times 2.5''$  module. In order to maximize the use of space in the PV-powered membrane system, the three elements in series were arranged vertically from top to bottom. Consequently, the pipes connecting adjacent elements were sharply curved, which caused flow disturbances and thus affected flow measurement [58, 59]. In addition, the tripled length of the flow path, the nearly tripled crossflow velocity, and the excessive number of endcaps in the  $3 \times 2.5''$  module could also contribute to the unstable flow readings. Nevertheless, such unstable readings could be tolerated since they did not shield the measurement under fluctuating solar conditions, which was the specific focus of this study.

The results of the SEC and permeate quality produced by the two modules of NF270 are presented in Figure 5. The SEC mainly depends on the salinity of the water, the permeability of the membrane, the configuration of the system, the recovery, and the efficiency of the pump [60, 61].

There was no markedly difference between the combined SEC of the  $3 \times 2.5''$  module and the SEC of the  $1 \times 4''$  module under maximum intensity of solar irradiance. However, the SEC of the  $3 \times 2.5''$  modules demonstrated more dramatic volatility during the heavy cloud periods, which were attributed to greater variations in the flux values (Figure 5B).

The  $1\times4''$  module showed an increase in EC from 2000 to 3000  $\mu$ S/cm during the light cloud period and from 2000 to 4000  $\mu$ S/cm during the heavy cloud period (Figure 5C). The increased salt concentration during cloudy periods was primarily attributed to the severe drop in flux resulting in less 'dilution'. Besides, the decline in feed flow reduced the crossflow velocity and thus probably facilitated salt diffusion across the membrane [10]. In the  $3\times2.5''$  module, the effect of energy fluctuation on permeate EC was drastic for the third element while the effect was rather moderate for the first two elements. As the available solar irradiance decreased from 1000 to 350 W/m², during the light cloud period, the permeate EC of the first element increased slightly from 1400 to 1800  $\mu$ S/cm, while the third element experienced a drastic increase from 2500 to 4500  $\mu$ S/cm (Figure 5D). During the heavy cloud period, the flux reached 0 L/m².h. The peak appearing at the end of the heavy cloud period was due to the washing away of permeate that remained in the system during this downtime.

The permeate F<sup>-</sup> and IC of both modules varied with solar irradiance in an analogous manner, which exhibited an abrupt peak during the heavy cloud period (Figure 5E–H). This was again because of the severe flux reduction. It is worthwhile mentioning that the permeate F<sup>-</sup> and IC of the third element of the 3× 2.5" module appears to be less affected by energy fluctuation, which seems inconsistent with the trend of the permeate EC. This is in fact due to the two different measurement methods of EC and F<sup>-</sup>/IC, namely in-line monitoring and manual water sampling [62]. The permeate EC was measured continuously by the in-line EC sensor, thereby the EC peaks were precisely recorded. The permeate F<sup>-</sup> and IC concentration, on the other hand, were measured intermittently from discrete samples (samples were taken every two minutes). Inevitably there was some unavoidable error in the peak positions and amplitudes.

Considering the flux, SEC and permeate quality, the performance of the first element of the  $3 \times 2.5''$  module was better than the  $1 \times 4''$  module. However, the deficient performance of the third element of the  $3 \times 2.5''$  module resulted in obtaining a similar overall performance compared to the  $1 \times 4''$  module.

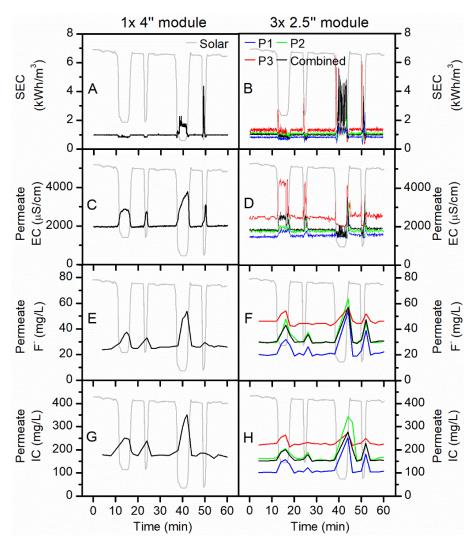


Figure 5 Comparison of the  $1 \times 4''$  and  $3 \times 2.5''$  modules of NF270 over 60 min of the solar day: (A, B) SEC, (C, D) permeate EC, (E, F) permeate F<sup>-</sup> concentration, (G, H) permeate IC concentration.

#### 3.4. Performance of the 1×4" and 3×2.5" modules of BW30 during cloudy periods

The effect of changing to a denser SW membrane with high salt retention, BW30, on the performance of the batteryless PV-powered system was studied as well. The results of the performance testing of the two configurations,  $1 \times 4''$  and  $3 \times 2.5''$  BW30 modules, are presented in Figure 6 and Figure 7. The pressure applied to both BW30 module types were nearly identical, as were the feed flows (Figure 6A–D). The unstable readings in feed flow and flux of the  $3 \times 2.5''$  module under steady-state conditions were attributed to flow disturbances, as explained earlier for NF270. Flux and recovery of the  $1 \times 4''$  module of BW30 was notably better than the  $3 \times 2.5''$  module (Figure 6E–H), which was attributed to a lower axial pressure drop and a lower hydraulic resistance. In consequence, the combined SEC of the  $3 \times 2.5''$  module was higher than that of the  $1 \times 4''$  module, let alone the extremely high SEC of the third element of the  $3 \times 2.5''$  module (Figure 7A,B). As discussed

above, the higher rejecting BW30 was more sensitive to axial pressure drop than the NF270 because of a higher osmotic pressure and thus a lower net driving pressure. Therefore the  $3 \times 2.5$ " module performed more poorly compared to the  $1 \times 4$ " module when using BW30.



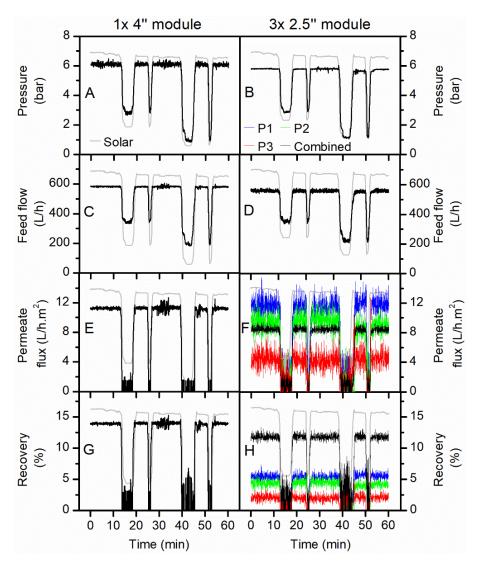


Figure 6 Comparison of the  $1 \times 4''$  and  $3 \times 2.5''$  modules of BW30 over 60 min of the solar day: (A, B) pressure, (C, D) feed flow, (E, F) flux, (G, H) recovery.

It is noteworthy that the flux values of both modules dropped to  $0 \text{ L/m}^2$ .h during the light and heavy cloud periods, which had a negative impact on the permeate quality. There was a spike in the permeate EC upon the end of every cloud period. The zero permeate EC reading during the heavy cloud period was because of air in the sensor (Figure 7C,D). The combined permeate EC of the  $3\times 2.5''$  module was lower than that of the  $1\times 4''$  module, due to the first and third elements of the  $3\times 2.5''$  module exhibiting remarkably efficient salt rejection (Figure 7D). In contrast, the third element

of the  $3 \times 2.5$ " module performed rather poorly in this respect.

Regarding F<sup>-</sup> and IC removal, the performance of 1× 4" module was better than the 3× 2.5" module (Figure 7E–H). When analyzing individual elements of the 3× 2.5" module, the first two elements of the 3× 2.5" module exhibited good removal efficiency while the third element was inefficient in this regard. In fact, the performance of the third element was so poor that it was hardly worth having this element present in the module. It is noteworthy that the permeate F<sup>-</sup> concentration of both modules temporarily exceeded the guideline value during the cloud periods. However, when considering that the permeate was continuously stored in a product tank, the system equipped with BW30 modules was able to produce safe drinking water in a long term, as will be discussed below.

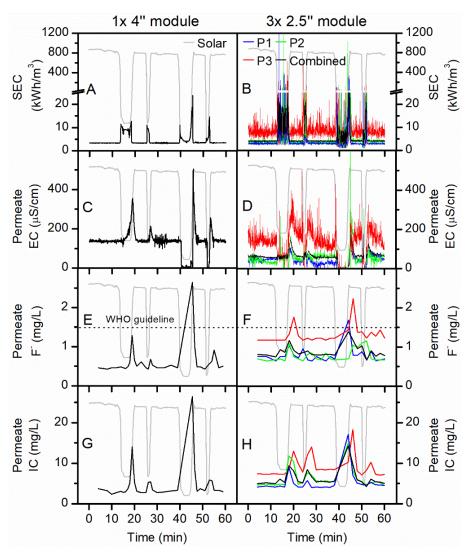


Figure 7 Comparison of the  $1 \times 4''$  and  $3 \times 2.5''$  modules of BW30 over 60 min of the solar day: (A, B) SEC, (C, D) permeate EC, (E, F) permeate F<sup>-</sup> concentration, (G, H) permeate IC concentration.

## 3.5. Overall comparison of the $1 \times 4$ " and $3 \times 2.5$ " modules

As discussed above, the performance of the 1× 4" and 3× 2.5" modules of the NF270 and BW30 membranes were evaluated and compared respectively during both cloudless and cloudy periods. The overall performances of these modules were characterized by two parameters: the first parameter is the cumulative sum of permeate water volume over time, which represents the productivity of the module; the second parameter is the cumulative sum of permeate F<sup>-</sup> concentration over time, which indicates the permeate quality when continuously collected in a tank. The results are shown in Figure 8, along with the results for two other 1× 4" modules (NF90 and BW30LE) and one 3× 2.5" module (XLE), for which the complete performance data are presented in the Supplementary Information. The flux for the first two 2.5" elements is higher (2 mg/L) than that of the 4" element (<1 mg/L). This is somewhat anomalous and because the XLE membrane is not usually included in this research no clear explanation for observation can be provided. Possibly this performance is due to a quality variation between the individual elements.

The cumulative permeate volume of all modules increased linearly with time, apart from during the cloud periods when the productivity was reduced for a short time (Figure 8A). In case of NF270, the permeate volumes produced by both modules were nearly the same (222 – 226 L), whereas for BW30 the  $1\times 4''$  module (63 L) produced a higher permeate volume than the  $3\times 2.5''$  module (52 L). The other three modules contained tight NF (NF90) and low energy RO (BW30LE, XLE) membranes. Their water productivities were around halfway between that of the loose NF (NF270) and the tight RO (BW30) membranes. The overall order was as follows:  $1\times 4''$  NF270 >  $3\times 2.5''$  NF270 >  $1\times 4''$  NF90 >  $3\times 2.5''$  XLE >  $1\times 4''$  BW30LE >  $1\times 4''$  BW30 >  $3\times 2.5''$  BW30, which was completely consistent with the order of the permeance values, as reported in Table 2.

The cumulative permeate F<sup>-</sup> concentration of all modules increased in a stepped manner due to the dramatic soar of transient concentration during the cloud periods (Figure 8B). It is evident that the  $1 \times 4$ " module had a better performance than the  $3 \times 2.5$ " module for both NF270 and BW30. As discussed above, the third element of the  $3 \times 2.5$ " module reduced the overall performance of the module significantly, which was due to the increasing feed concentration and the greater pressure drop along the feed channel. The cumulative permeate F<sup>-</sup> concentration of all modules followed the order:  $3 \times 2.5$ " NF270 >  $1 \times 4$ " NF270 >  $3 \times 2.5$ " XLE >  $1 \times 4$ " NF90 >  $1 \times 4$ " BW30LE >  $3 \times 2.5$ " BW30 >  $1 \times 4$ " BW30. The order of membrane type was in good agreement with the salt rejection data provided by the manufacturer [63]. Even though the cloudy periods did not contribute substantially to water quality in this study, when longer cloud periods are experienced and

consequently the transients are even longer this contribution may need to be controlled to not compromise the overall water quality. Long term tests will be required to evaluate this and the control algorithm and hardware may be expanded to include a permeate flush for such periods.

When refering to the WHO guideline limit for F<sup>-</sup> concentration of 1.5 mg/L, three 1× 4" modules (1× 4" BW30, 1× 4" BW30LE and 1× 4" NF90) and one 3× 2.5" module (3× 2.5" BW30) were able to meet the guideline throughout the 60-min period. The other three modules (3× 2.5" NF270, 1× 4" NF270, and 3× 2.5" XLE), on the contrary, failed to produce permeate with acceptable F<sup>-</sup> concentrations. It should be noted that XLE, as a RO membrane, was designed to have a higher salt rejection than NF90 [63]. The inferior F<sup>-</sup> removal of 3× 2.5" XLE compared to 1× 4" NF90 revealed the significant impact of module size on the actual system performance. The 1× 4" NF90 module seemed to be the best option in balancing permeate productivity and quality, which produced 127 L of drinking water with 1.2 mg/L F<sup>-</sup> within the 60-min period.

When it comes to the cost factor, the market price of three 2.5'' elements is much higher than that of one 4" element, let alone the extra associated costs for three elements, such as extra tubing and pressure vessels. It is thus more cost-effective to use the  $1\times4''$  module rather than the  $3\times2.5''$  module.

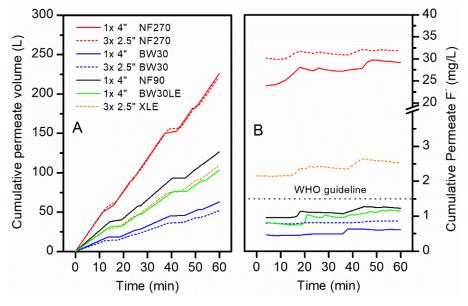


Figure 8 Comparison of cumulative (A) permeate volume and (B) permeate  $F^-$  concentration for different  $1 \times 4''$  and  $3 \times 2.5''$  modules over 60 min of the solar day.

#### 4. Conclusions

This study investigated the impact of membrane module size on the performance of a batteryless PV-powered membrane system under fluctuating solar conditions. Several NF/RO

membranes in two module sizes  $(1 \times 4'')$  and  $3 \times 2.5''$ ) of the same membrane area were used to treat a naturally fluoridated brackish water in a remote village in northern Tanzania.

Under steady-state conditions, the  $1\times 4''$  and  $3\times 2.5''$  modules of NF270 achieved good flux  $(33-35 \text{ L/m}^2\text{.h})$  and SEC  $(0.98 \text{ kWh/m}^3)$ , but as expected, the permeate quality  $(25-30 \text{ mg/L F}^-)$  was too poor to meet the drinking water guideline for fluoride. Meanwhile the  $1\times 4''$  and  $3\times 2.5''$  modules of BW30 exhibited much lower flux  $(8-12 \text{ L/m}^2\text{.h})$  and correspondingly a higher SEC  $(3-4 \text{ kWh/m}^3)$ , but the permeate F<sup>-</sup> concentration (0.5-0.8 mg/L) was satisfactory for drinking purposes.

Under fluctuating solar conditions, the pressure and feed flow of the modules decreased drastically, thus reducing the flux and increasing the SEC. The permeate water quality degraded sharply because of the severe drop in flux. The transient permeate F<sup>-</sup> concentration of BW30 modules temporarily exceeded the guideline value. However, if being collected in a product tank, the cumulative permeate F<sup>-</sup> concentration of BW30 could always meet the WHO drinking water guideline. The NF90 and BW30LE modules also achieved very good performance.

The performance of the  $1\times 4''$  module was always equivalent to or better than that of the  $3\times 2.5''$  module of the same membrane. This was mainly because the third element of the  $3\times 2.5''$  module decreased the overall performance of the module substantially. Taking into account the cost factor, large diameter SW modules enable considerable reductions in capital cost and life-cycle cost, thereby increasing the economic feasibility of implementing PV-powered membrane systems in remote and rural locations. Future work will focus on development of appropriate modelling frameworks for performance simulation of PV-powered membrane systems during both steady-state and fluctuating operations.

# 5. Acknowledgements

The research was funded in part by two Leverhulme Royal Society Africa Awards SADWAT-Tanzania and SUCCESS; as well as the Helmholtz Association Recruitment Initiative for AIS and BSR. The Energy Technology Partnership (ETP) and Drinking Water Quality Regulator for Scotland (DWQR) provided the PhD scholarship for JS. The DOW Chemical Company kindly donated the NF/RO membrane modules for this project, and GE Power & Water (Zenon) the UF module. Godfrey Mkongo (Ngurdoto Defluoridation Research Station (NDRS), Tanzania) is greatly appreciated for his hospitality when carrying out experiments at NDRS. William Dahi (Defluoridation Technology Project, Tanzania) carried out the analysis of a huge number of samples, while Elly Karle and Reinhard Sembritzki (KIT, Germany) provided IC and ICP data the source water sample. Minh

- Nguyen (KIT, Germany) is thanked for drawing the graphic of the spiral wound element in the SI.
- Prof Jack Gilron (BGU, Israel) has inspired this work through his questions at the PhD defense of
- 573 Gavin Park.

575

# 6. Supplementary Information

- The SI contains a schematic of a spiral wound module, as well as further data of the NF90,
- 577 BW30LE and XLE membranes.

#### **7. References**

- 579 [1] J. Alcamo, N. Fernandez, S.A. Leonard, P. Peduzzi, A. Singh, R. Harding Rohr Reis, 21 issues
- for the 21st Century: results of the UNEP Foresight Process on Emerging Environmental issues,
- 581 (2012).
- 582 [2] B.S. Richards, J. Shen, A.I. Schäfer, Water-energy nexus perspectives in the context of
- 583 photovoltaic-powered decentralized water treatment systems: A Tanzanian case study, Energy
- 584 Technology, (2017) 1-13.
- [3] A.I. Schäfer, A. Broeckmann, B.S. Richards, Renewable Energy Powered Membrane Technology.
- 1. Development and Characterization of a Photovoltaic Hybrid Membrane System, Environmental
- 587 Science & Technology, 41 (2007) 998-1003.
- [4] V.G. Gude, N. Nirmalakhandan, S. Deng, Renewable and sustainable approaches for desalination,
- Renewable and Sustainable Energy Reviews, 14 (2010) 2641-2654.
- 590 [5] M. Shatat, M. Worall, S. Riffat, Opportunities for solar water desalination worldwide: Review,
- 591 Sustainable Cities and Society, 9 (2013) 67-80.
- 592 [6] D. Herold, A. Neskakis, A small PV-driven reverse osmosis desalination plant on the island of
- 593 Gran Canaria, Desalination, 137 (2001) 285-292.
- 594 [7] M. Thomson, D. Infield, A photovoltaic-powered seawater reverse-osmosis system without
- 595 batteries, Desalination, 153 (2003) 1-8.
- [8] A. Chafidz, E.D. Kerme, I. Wazeer, Y. Khalid, A. Ajbar, S.M. Al-Zahrani, Design and fabrication
- of a portable and hybrid solar-powered membrane distillation system, Journal of Cleaner Production,
- 598 133 (2016) 631-647.
- 599 [9] S.M. Shalaby, Reverse osmosis desalination powered by photovoltaic and solar Rankine cycle
- power systems: A review, Renewable and Sustainable Energy Reviews, 73 (2017) 789-797.
- [10] J. Shen, B.S. Richards, A.I. Schäfer, Renewable energy powered membrane technology: Case
- study of St. Dorcas borehole in Tanzania demonstrating fluoride removal via nanofiltration/reverse
- osmosis, Separation and Purification Technology, 170 (2016) 445-452.
- 604 [11] A. Joyce, D. Loureiro, C. Rodrigues, S. Castro, Small reverse osmosis units using PV systems
- for water purification in rural places, Desalination, 137 (2001) 39-44.

- 606 [12] T. Espino, B. Peñate, G. Piernavieja, D. Herold, A. Neskakis, Optimised desalination of seawater
- by a PV powered reverse osmosis plant for a decentralised coastal water supply, Desalination, 156
- 608 (2003) 349-350.
- [13] M.A. Alghoul, P. Poovanaesvaran, M.H. Mohammed, A.M. Fadhil, A.F. Muftah, M.M. Alkilani,
- K. Sopian, Design and experimental performance of brackish water reverse osmosis desalination unit
- powered by 2 kW photovoltaic system, Renewable Energy, 93 (2016) 101-114.
- [14] B.S. Richards, D.P.S. Capão, A.I. Schäfer, Renewable energy powered membrane technology.
- 2. The effect of energy fluctuations on performance of a photovoltaic hybrid membrane system,
- 614 Environmental Science & Technology, 42 (2008) 4563-4569.
- 615 [15] E.S. Mohamed, G. Papadakis, E. Mathioulakis, V. Belessiotis, A direct coupled photovoltaic
- 616 seawater reverse osmosis desalination system toward battery based systems a technical and
- economical experimental comparative study, Desalination, 221 (2008) 17-22.
- [16] M. Thomson, D. Infield, Laboratory demonstration of a photovoltaic-powered seawater reverse-
- osmosis system without batteries, Desalination, 183 (2005) 105-111.
- 620 [17] B.S. Richards, D.P.S. Capão, W.G. Früh, A.I. Schäfer, Renewable energy powered membrane
- 621 technology: Impact of solar irradiance fluctuations on performance of a brackish water reverse
- osmosis system, Separation and Purification Technology, 156, Part 2 (2015) 379-390.
- [18] L.A. Richards, B.S. Richards, A.I. Schäfer, Renewable energy powered membrane technology:
- 624 Salt and inorganic contaminant removal by nanofiltration/reverse osmosis, Journal of Membrane
- 625 Science, 369 (2011) 188-195.
- 626 [19] Dow Water and Process Solutions, FILMTEC<sup>TM</sup> Reverse Osmosis Membranes Technical
- 627 Manual,
- 628 http://msdssearch.dow.com/PublishedLiteratureDOWCOM/dh 095b/0901b8038095b91d.pdf?filepa
- 629 th=/609-00071.pdf&fromPage=GetDoc. Access date: May.
- [20] J. Shen, G. Mkongo, G. Abbt-Braun, S.L. Ceppi, B.S. Richards, A.I. Schäfer, Renewable energy
- powered membrane technology: Fluoride removal in a rural community in northern Tanzania,
- 632 Separation and Purification Technology, 149 (2015) 349-361.
- [21] J. Schwinge, P.R. Neal, D.E. Wiley, D.F. Fletcher, A.G. Fane, Spiral wound modules and spacers:
- Review and analysis, Journal of Membrane Science, 242 (2004) 129-153.
- 635 [22] A.J. Karabelas, M. Kostoglou, C.P. Koutsou, Modeling of spiral wound membrane desalination
- modules and plants review and research priorities, Desalination, 356 (2015) 165-186.
- [23] J. Johnson, M. Busch, Engineering aspects of reverse osmosis module design, Desalination and
- 638 Water Treatment, 15 (2010) 236-248.
- 639 [24] A.J. Karabelas, C.P. Koutsou, M. Kostoglou, The effect of spiral wound membrane element
- design characteristics on its performance in steady state desalination A parametric study,
- 641 Desalination, 332 (2014) 76-90.
- [25] J. Fawell, K. Bailey, J. Chilton, E. Dahi, L. Fewtrell, Y. Magara, Fluoride in drinking water,
- World Health Organization, London 2006.

- [26] J.P. Shorter, J. Massawe, N. Parry, R.W. Walker, Comparison of two village primary schools in
- northern Tanzania affected by fluorosis, International Health, 2 (2010) 269-274.
- 646 [27] H.G. Jarvis, P. Heslop, J. Kisima, W.K. Gray, G. Ndossi, A. Maguire, R.W. Walker, Prevalence
- and aetiology of juvenile skeletal fluorosis in the south-west of the Hai district, Tanzania a
- community-based prevalence and case-control study, Tropical Medicine & International Health, 18
- 649 (2013) 222-229.
- 650 [28] H. Mjengera, G. Mkongo, Appropriate deflouridation technology for use in flourotic areas in
- Tanzania, Physics and Chemistry of the Earth, 28 (2003) 1097-1104.
- [29] S. Ayoob, A.K. Gupta, V.T. Bhat, A conceptual overview on sustainable technologies for the
- defluoridation of drinking water, Critical Reviews in Environmental Science and Technology, 38
- 654 (2008) 401-470.
- [30] K.M.K. Kut, A. Sarswat, A. Srivastava, C.U. Pittman, D. Mohan, A review of fluoride in african
- 656 groundwater and local remediation methods, Groundwater for Sustainable Development, 2-3 (2016)
- 657 190-212.
- 658 [31] J. Shen, A.I. Schäfer, Factors affecting fluoride and natural organic matter (NOM) removal from
- 659 natural waters in Tanzania by nanofiltration/reverse osmosis, Science of The Total Environment,
- 660 527–528 (2015) 520-529.
- 661 [32] C. Onorato, M. Gaedtke, M. Kespe, H. Nirschl, A.I. Schäfer, Renewable energy powered
- membrane technology: computational fluid dynamics evaluation of system performance with variable
- module size and fluctuating energy, Separation and Purification Technology, (2019).
- 664 [33] World Health Organization, Guidelines for drinking-water quality: fourth edition incorporating
- the first addendum, in, Geneva, 2017.
- [34] A.I. Schäfer, A. Broeckmann, B.S. Richards, Renewable energy powered membrane technology.
- 1. development and characterization of a photovoltaic hybrid membrane system, Environmental
- 668 Science & Technology, 41 (2006) 998-1003.
- 669 [35] B.S. Richards, G.L. Park, T. Pietzsch, A.I. Schäfer, Renewable energy powered membrane
- 670 technology: Brackish water desalination system operated using real wind fluctuations and energy
- buffering, Journal of Membrane Science, 468 (2014) 224-232.
- [36] Dow Chemical Company, DOW FILMTEC Fiberglassed Elements for Light Industrial Systems,
- 673 <a href="http://www.dupont.com/content/dam/Dupont2.0/Products/water/literature/609-00350.pdf">http://www.dupont.com/content/dam/Dupont2.0/Products/water/literature/609-00350.pdf</a>. Access
- 674 date: 12 November 2018.
- 675 [37] Dow Chemical Company, FILMTEC Membranes NF270 Nanofiltration Elements for
- 676 Commercial Systems,
- 677 http://www.dupont.com/content/dam/Dupont2.0/Products/water/literature/609-00519.pdf. Access
- 678 date: 12 November 2018.
- 679 [38] Dow Chemical Company, DOW FILMTEC Membranes DOW FILMTEC NF90 Nanofiltration
- 680 Elements for Commercial Systems,
- 681 <a href="http://www.dupont.com/content/dam/Dupont2.0/Products/water/literature/609-00378.pdf">http://www.dupont.com/content/dam/Dupont2.0/Products/water/literature/609-00378.pdf</a>. Access
- 682 date: 12 November 2018.

- [39] Dow Chemical Company, FILMTEC Membranes Basics of RO and NF: Element Characteristics,
- http://msdssearch.dow.com/PublishedLiteratureDOWCOM/dh 0071/0901b803800710df.pdf.
- Access date: 12 November 2018.
- 686 [40] Dow Chemical Company, FILMTEC Membranes System Design: Introduction,
- 687 <a href="http://msdssearch.dow.com/PublishedLiteratureDOWCOM/dh\_0043/0901b803800435bd.pdf?filepa">http://msdssearch.dow.com/PublishedLiteratureDOWCOM/dh\_0043/0901b803800435bd.pdf?filepa</a>
- 688 <u>th=liquidseps/pdfs/noreg/609-02046.pdf.</u> Access date: 12 November 2018.
- 689 [41] Dow Chemical Company, FILMTEC XLE-2540 Membranes Extra Low Energy Elements for
- 690 Commercial Systems,
- 691 <a href="http://www.dupont.com/content/dam/Dupont2.0/Products/water/literature/609-00349.pdf">http://www.dupont.com/content/dam/Dupont2.0/Products/water/literature/609-00349.pdf</a>. Access
- 692 date: 12 November 2018.
- 693 [42] Dow Chemical Company, FILMTEC LE-4040 Membranes Fiberglassed Elements for Light
- Industrial Systems, https://www.lenntech.com/Data-sheets/Dow-Filmtec-LE-4040.pdf. Access date:
- 695 12 November 2018.
- 696 [43] B.S. Richards, G.L. Park, T. Pietzsch, A.I. Schäfer, Renewable energy powered membrane
- 697 technology: Safe operating window of a brackish water desalination system, Journal of Membrane
- 698 Science, 468 (2014) 400-409.
- 699 [44] A.I. Schäfer, J. Shen, B.S. Richards, Renewable energy powered membrane technology:
- Removal of natural organic matter and fluoride in Tanzanian communities, npj Nature Clean Water,
- 701 24 (2018) 1-10.
- 702 [45] A.F. Derradji, S. Taha, G. Dorange, Application of the resistances in series model in
- 703 ultrafiltration, Desalination, 184 (2005) 377-384.
- 704 [46] G. Schock, A. Miguel, Mass transfer and pressure loss in spiral wound modules, Desalination,
- 705 64 (1987) 339-352.
- 706 [47] J. Mulder, Basic Principles of Membrane Technology, Springer, Netherlands, 1996.
- 707 [48] I.E. Idelchik, Handbook of Hydraulic Resistance, Begell House Publishers, USA, 2007.
- 708 [49] MathWorks, Hydraulic resistance in pipe bend,
- 709 https://www.mathworks.com/help/physmod/hydro/ref/pipebend.html. Access date: 12 November
- 710 2018.
- 711 [50] K. Boussu, Y. Zhang, J. Cocquyt, P. Van der Meeren, A. Volodin, C. Van Haesendonck, J.A.
- 712 Martens, B. Van der Bruggen, Characterization of polymeric nanofiltration membranes for systematic
- analysis of membrane performance, Journal of Membrane Science, 278 (2006) 418-427.
- 714 [51] I. Owusu-Agyeman, A. Jeihanipour, T. Luxbacher, A.I. Schäfer, Implications of humic acid,
- 715 inorganic carbon and speciation on fluoride retention mechanisms in nanofiltration and reverse
- osmosis, Journal of Membrane Science, 528 (2017) 82-94.
- 717 [52] H. Choi, K. Zhang, D.D. Dionysiou, D.B. Oerther, G.A. Sorial, Influence of cross-flow velocity
- on membrane performance during filtration of biological suspension, Journal of Membrane Science,
- 719 248 (2005) 189-199.

- 720 [53] J.S. Vrouwenvelder, C. Picioreanu, J.C. Kruithof, M.C.M. van Loosdrecht, Biofouling in spiral
- wound membrane systems: Three-dimensional CFD model based evaluation of experimental data,
- 722 Journal of Membrane Science, 346 (2010) 71-85.
- 723 [54] J. Luo, Y. Wan, Effects of pH and salt on nanofiltration A critical review, Journal of Membrane
- 724 Science, 438 (2013) 18-28.
- 725 [55] S.M.J. Zaidi, F. Fadhillah, Z. Khan, A.F. Ismail, Salt and water transport in reverse osmosis thin
- film composite seawater desalination membranes, Desalination, 368 (2015) 202-213.
- 727 [56] Y. Marcus, Thermodynamics of solvation of ions. Part 5.-Gibbs free energy of hydration at
- 728 298.15 K, Journal of the Chemical Society, Faraday Transactions, 87 (1991) 2995-2999.
- 729 [57] L.A. Richards, B.S. Richards, B. Corry, A.I. Schäfer, Experimental energy barriers to anions
- transporting through nanofiltration membranes, Environmental Science & Technology, 47 (2013)
- 731 1968-1976.
- 732 [58] Seametrics, Resolving flowmeter instability problems, in, USA, 2009.
- 733 [59] G.H. Keulegan, K.H. Beij, Pressure Losses for Fluid Flow in Curved Pipes, US Government
- 734 Printing Office, USA, 1937.
- 735 [60] H.M. Laborde, K.B. França, H. Neff, A.M.N. Lima, Optimization strategy for a small-scale
- reverse osmosis water desalination system based on solar energy, Desalination, 133 (2001) 1-12.
- 737 [61] C. Charcosset, A review of membrane processes and renewable energies for desalination,
- 738 Desalination, 245 (2009) 214-231.
- 739 [62] G.J. Kirmever, Guidance Manual for Monitoring Distribution System Water Quality, American
- 740 Water Works Association, USA, 2002.
- 741 [63] Dow Chemical Company, Dow Water and Process Solutions Levels of Separation of IX, RO,
- NF, UF, https://dowwater.custhelp.com/app/answers/detail/a id/477. Access date: 12 November
- 743 2018.

/46	SUPPLEMENTARY INFURMATION
747	
748	Renewable energy powered membrane technology: experimental
749	investigation of system performance with variable module size and fluctuating
750	energy
751	
752	Junjie Shen <sup>1,2,3</sup> , Azam Jeihanipour <sup>4</sup> , Bryce S. Richards <sup>2,4</sup> , Andrea I. Schäfer <sup>3,5*</sup>
753	
754	<sup>1</sup> Centre for Advanced Separations Engineering, University of Bath, Bath BA2 7AY,
755	United Kingdom
756	<sup>2</sup> School of Engineering and Physical Sciences, Heriot-Watt University, Edinburgh
757	EH14 4AS, United Kingdom
758	<sup>3</sup> Water and Environmental Science and Engineering, Nelson Mandela African Institute of
759	Science and Technology, Arusha, Tanzania
760	<sup>4</sup> Institute of Microstructure Technology (IMT), KIT, Hermann-von-Helmholtz-Platz 1,
761	76344 Eggenstein-Leopoldshafen, Germany
762	<sup>5</sup> Membrane Technology Department, Institute of Functional Interfaces (IFG-MT),
763	Karlsruhe Institute of Technology, Hermann-von-Helmholtz-Platz 1, 76344 Eggenstein-
764	Leopoldshafen, Germany
765	
766	
767	
768	
769	
770	
771	
772	
773	
774	
775	
776	
777	
778	



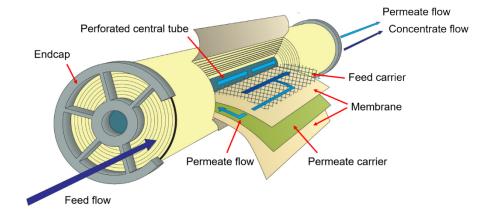


Figure S1 Graphic of a spiral wound element

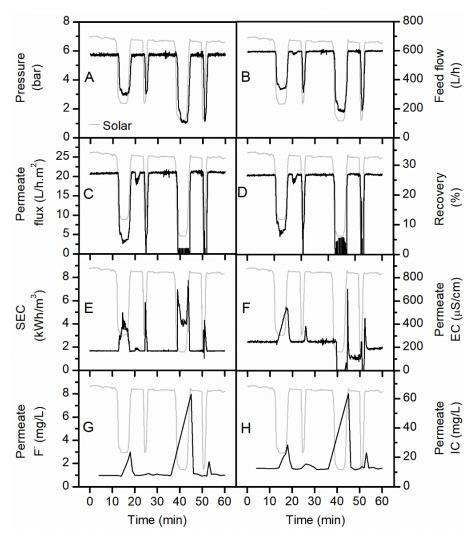


Figure S2 Instantaneous system performance of  $1 \times 4''$  NF90 module over 60 min of the solar day: (A) pressure, (B) feed flow, (C) flux, (D) recovery, (E) SEC, (F) permeate EC, (G) permeate F-concentration, (H) permeate IC concentration

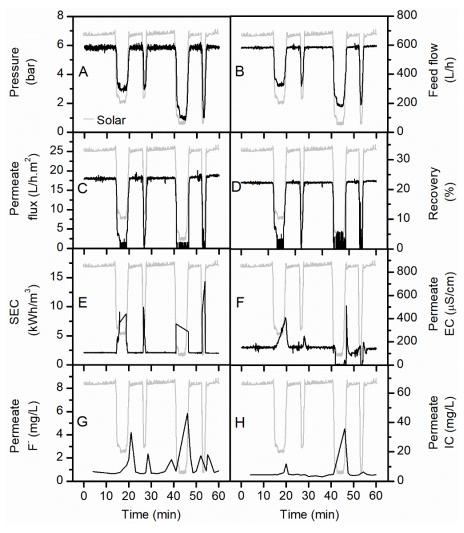


Figure S3 Instantaneous system performance of  $1 \times 4''$  BW30LE module over 60 min of the solar day: (A) pressure, (B) feed flow, (C) flux, (D) recovery, (E) SEC, (F) permeate EC, (G) permeate F<sup>-</sup> concentration, (H) permeate IC concentration

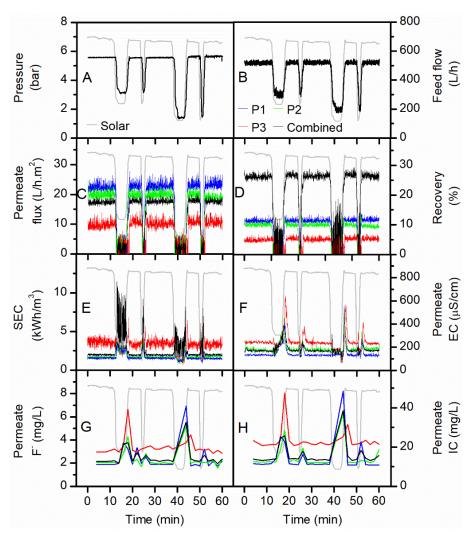


Figure S4 Instantaneous system performance of 3× 2.5" XLE module over 60 min of the solar day: (A) pressure, (B) feed flow, (C) flux, (D) recovery, (E) SEC, (F) permeate EC, (G) permeate F-concentration, (H) permeate IC concentration